ACS OMEGA

Open Access

http://pubs.acs.org/journal/acsodf

Review

Liquid Marbles and Drops on Superhydrophobic Surfaces: Interfacial Aspects and Dynamics of Formation: A Review

Apoorva Sneha Ravi and Sameer Dalvi*

Cite This: *ACS Omega* 2024, 9, 12307−12330

Read Online

ACCESS | Metrics & More | Article Recommendations

ABSTRACT: Liquid marbles (LMs) are droplets encapsulated with powders presenting varied roughness and wettability. These LMs have garnered a lot of attention due to their dual properties of leakage-free and quick transport on both solid and liquid surfaces. These droplets are in a Cassie−Baxter wetting state sitting on both roughness and air pockets existing between particles. They are also reminiscent of the state of a drop on a superhydrophobic (SH) surface. In this review, LMs and bare droplets on SH surfaces are comparatively investigated in terms of two aspects: interfacial and dynamical. LMs present a fascinating class of soft matter due to their superior interfacial activity and their remarkable stability. Inherently hydrophobic powders form stable LMs by simple rolling; however, particles with defined morphologies and chemistries contribute to the varied stability of LMs. The factors contributing to this interesting robustness with respect to bare droplets are then identified by tests of stability such as evaporation and compression. Next, the dynamics of the impact of a drop on a hydrophobic powder bed to form LMs is studied vis-à-vis that of drop impact on flat surfaces. The knowledge from drop impact phenomena on flat surfaces is used to build and complement insights to that of drop impact on powder surfaces. The maximum spread of the drop is empirically understood in terms of dimensionless numbers, and their drawbacks are highlighted. Various stages of drop impact—spreading, retraction and rebound, splashing, and final outcome—are systematically explored on both solid and hard surfaces. The implications of crater formation and energy dissipations are discussed in the case of granular beds. While the drop impact on solid surfaces is extensively reviewed, deep interpretation of the drop impact on granular surfaces needs to be improved. Additionally, the applications of each step in the sequence of drop impact phenomena on both substrates are also identified. Next, the criterion for the formation of peculiar jammed LMs was examined. Finally, the challenges and possible future perspectives are envisaged.

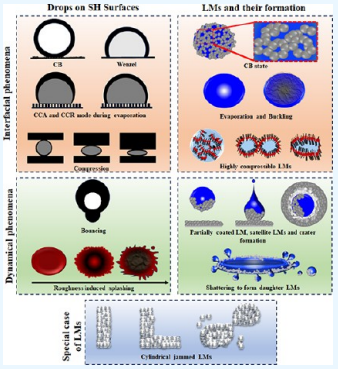

1. INTRODUCTION

Liquid marbles (LMs) are liquid droplets encapsulated with hydrophobic particles[1] or aggregates of hydrophilic particles.[2] The discovery of LMs started off with the pioneering work of Aussillous and Quéré[1] where the idea to transport small volumes of liquid easily without any leakage was envisaged. Plant-based lycopodium particles were used to enwrap millimeter-sized liquid droplets which formed LMs. A range of particles and liquids with varied sizes and volumes have been used to produce LMs.[3] LMs can be composed of both multilayers as well as monolayers based on the arrangement and method of preparation.[4−6] LMs are nonwetting, contamination-free, and stable to evaporation as compared to bare droplets.[7] They can also be transported onto liquid substrates where they remain stable.[8,9] LMs are recognized as a highly versatile class of soft matter as they can be compressed,[10] evaporated,[11] divided,[12] or coalesced[13] based on the nature of the application.

Examples of LMs and drops on superhydrophobic (SH) surfaces in nature are described. Gall-dwelling aphids parcel their excreta using secreted hydrophobic wax particles forming LMs (Figure 1a,b). This secreted wax is not only hydrophobic but also possesses an inherent roughness,[14] which leads to the formation of a Cassie−Baxter (CB) state.[15] The imaging of these microstructures revealed the organization of wax tufts into fibrous and dumpling-shaped assemblies[16] (Figure 1c−e). Powders impart nonwetting and rolling behavior to LMs akin to that of drops on SH surfaces with hierarchical architecture. For example, lotus leaves have a two-tier roughness containing papillose epidermal cells and a layer of epicuticular waxes, which lead to enhanced superhydrophobicity and facilitate rolling away from the surface.[17]

The recent applications of LMs by manipulation of their components are discussed. Stimuli-responsive LMs can be designed to rupture at specific points either by changing the surface tension of liquid[18] or tuning the wettability of shell.[19]

Received: October 3, 2023
Revised: February 12, 2024
Accepted: February 14, 2024
Published: March 5, 2024

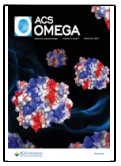

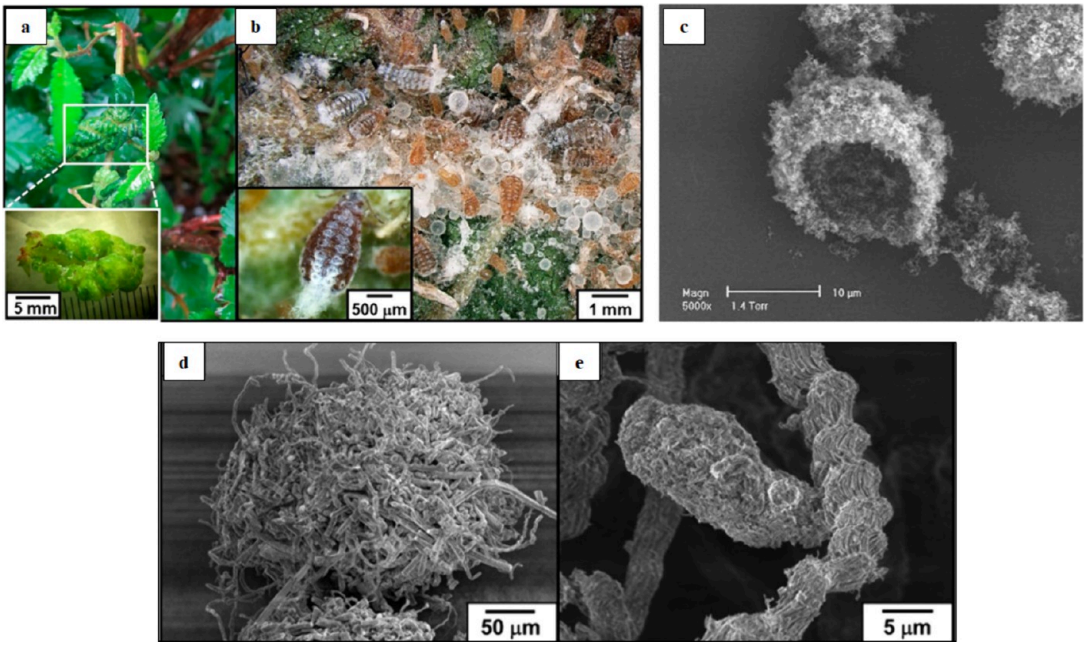

Figure 1. LMs in nature. (a) Gall fabricated by an aphid. The inset is a magnified image of this structure. (b) Imaging of internal gall showing numerous LMs. The inset shows the secreted wax on aphid's body. (c) Electron microscopy of LM fabricated by aphids. (d–e) Dumpling and fiber-shaped particle assemblies adsorbed at the LM surface. Reprinted with permission from ref 16. Copyright 2019 American Chemical Society.

Further, LMs can be propelled by tailoring shell material or the vaporizability of the core liquid.[20−22] Floating LMs generate the formation of healthy 3D spheroids as compared to conventionally used techniques due to their spherical nature and buoyancy.[23] Various types of cells could be cultured inside a single millimetric LM for studying their interaction similar to that of a tissue microenvironment.[24] On the other hand, stationary LMs are used to miniaturize reactions such as blood-typing and methylene blue reduction, thus saving the amount of reagent used.[25,26] Moreover, the porous structure of the LM shell can aid in gas exchange with the outer environment, thus indicating its capability as a qualitative sensor.[27,28]

Coming to the preparation of LMs, rolling of droplets on powders is the predominantly used procedure.[8,29] Though the synthesis of LMs by rolling is simple, it cannot be used for their uniform coating.[30] On the other hand, industrial applications involve high-energy mixing of large quantities of water and hydrophobic particles at a particular ratio to prepare "dry water".[31,32] Drop impact on powder beds has been used to form coated LMs by prerequisite knowledge of drop spreading on flat surfaces.[33] The maximum spread ratio is an indicator of how the kinetic energy of a droplet is converted into surface energy and various dissipations associated with the liquid and the granular bed.[30,33,34] Insights based on dimensionless numbers show a wide variety of scaling, and their drawbacks are discussed. The various steps in drop impact phenomena of both flat and granular surfaces are then elaborated and scrutinized, leading to possible future research.

Reviews in the literature have focused on the fundamentals coupling statics and dynamics[35] and properties and applications of LMs with reference to other emerging soft matter systems.[36] Next, the stimuli-responsive feature of LMs and their promising potential in terms of microreactors were discussed.[37,38] In addition, an extensive summary of types of particles and liquids, as well as applications, was reported.[38−41] Recently, the concepts of capillarity and the surface tension-related aspects of LMs were also revisited.[42] Though a repository of particles, liquids, and applications was extensively reviewed, the lack of a one-to-one comparison between LMs and drops on SH surfaces is yet to be summarized.

In this review, efforts were made to assess LMs and drops on SH surfaces associated with the background of interfacial and dynamical aspects. First, the interfacial aspects of LMs vis-à-vis that of a drop on SH surfaces is analyzed. The energetics of particle adsorption and capillary forces contributing to their stability are understood in detail. LMs are known to show superior stability as compared to bare droplets due to their isolated environment and multilayer coating. Next, the phenomena of droplet impact on the granular surface were investigated vis-à-vis that of a flat surface. Various steps in droplet impact were then outlined on both types of surfaces, and their applications were also ascertained. Lastly, the critical threshold for frozen LMs was also inspected.

2. INTERFACIAL PROPERTIES OF LMs

2.1. Particle−Liquid and Particle−Particle Interactions. The understanding of interparticle forces first came into the picture with the formation of particle-stabilized emulsions. Surfactants are commonly used to stabilize emulsions because of their amphiphilic character; however, the stability is limited. The use of solid particles for stabilizing foams and emulsions started with the pioneering work of Pickering and Ramsden.[43,44] There was an enhancement in stability as compared to conventional surfactants. A particle will decrease the energy of the interface as it makes a hole in the fluid−fluid interface, thus reducing the contact area of the two fluids.[45] The size of this "hole" is determined by its CA or its wettability with the interface. The equation for minimization of energy[46] is as follows

$$\Delta E = -\pi r^2 \gamma_o (1 \pm \cos\theta)^2 \quad (1)$$

https://doi.org/10.1021/acsomega.3c07657
ACS Omega 2024, 9, 12307−12330

Table 1. Summary of Various Effective Surface Tension Methods

Sl. no.	type of method	formula	mechanism	advantages	disadvantages
1.	Puddle maximum height[53,66,67]	$\gamma_{\text{eff}}^{\theta} = \frac{\rho g h_{\max}^2}{4 \sin^2\left(\frac{\theta_{\text{LM}}}{2}\right)}$ where $\gamma_{\text{eff}}^{\theta}$ is the effective surface tension, ρ and g represent the density and gravity, respectively, $h_{\max}$ is the maximum height of the puddle ,and θ_{LM} is the macroscopic CA of this puddle-sized LM.	Height of a large puddle related to balance between surface tension and gravity	Simple and easily estimated	(a) Hard to measure exact position of three phase contact line. (b) Wettability of the substrate may lead to fluctuation of macroscopic contact angle of LM. (c) The right and left sides of LM may show CAs with deviation due to variation in areal density
2.	Pendant drop[55,62]	$\gamma\left(\frac{1}{R_1} + \frac{1}{R_2}\right) = \rho g z$ where ρ is the density of liquid, g is the gravity acceleration, R_1 and R_2 are the main radii of curvature of the pendant droplet surface with an axis as z.	Shape of a drop dictated by a balance of gravity and surface tension	(a) Easily coupled with surface tension of bare liquid interfaces. (b) Information about particles that exhibit strong interactions	(a) Multilayer of LMs hinders correct fitting of curve and detection. (b) Subject to any volume changes
3.	Vibration[53,54]	$\omega = \sqrt{2\pi\gamma h(\theta)(1 - \cos\theta)/\rho V}$ where ω is the resonant frequency, $h(\theta)$ is the geometrical factor,[68] ρ is the density, and V is the volume of the LM.	Relation of surface tension with resonant frequency	Sensitive to type of particle used	(a) LM should maintain sphericity and be pinned to substrate before vibration. (b) Should not roll off during measurement
4.	Capillary rise[56,60]	$\frac{\gamma_m}{m} = \rho g \Delta h_m$ where γ_m is the effective surface tension, ρ is the water density, g is the gravitational force, Δh_m is the additional capillary rise caused by the water marble, and $\frac{1}{m}$is the hydraulic radius of LM.	Near-spherical water/powder interface of the marble shell exerts a Laplace pressure	(a) Does not require measurement of contact angle with solid surface (b) Measuring γ_{eff} at any particle coverage	Handling capillary and accurate measurement of rise in thin tubes
5.	Wilhelmy plate[56,69,70]	$\gamma_{\text{w}} = \frac{F \cos\theta}{2(1 + t)}$ where γ_{w} and θ are the surface tension of water and the CA between water and the coverslip, respectively; l and t are the width and the thickness of the glass coverslip, respectively.	Advancing and receding action of a plate on a liquid surface coated with particles	Robust and simple measurement for studying particle arrangement behavior	(a) Sensitive to homogeneity of particles (b) Disturbance of the particle−water interface (c) Values dependent on size of particle and dooes not include multilayers
6.	Oscillating sessile LM[57]	$f_{\text{n}}^2 = \frac{\pi k^3 \gamma}{4\rho p^3}$ where f_{n} is the frequency, k is the number of nodes of the standing wave on the surface of the oscillating liquid marble, ρ is the effective density of the liquid marble, and p is the perimeter of the liquid marble profile.	Using natural oscillation of a sessile LM	(a) Noncontact mode (b) Increased consistency in values, no requirement of sphericity of LMs, no contact angle measurement	(a) Risk of interfacial jamming (b) More studies on viscosity, elasticity, and robustness

https://doi.org/10.1021/acsomega.3c07657
ACS Omega 2024, 9, 12307−12330

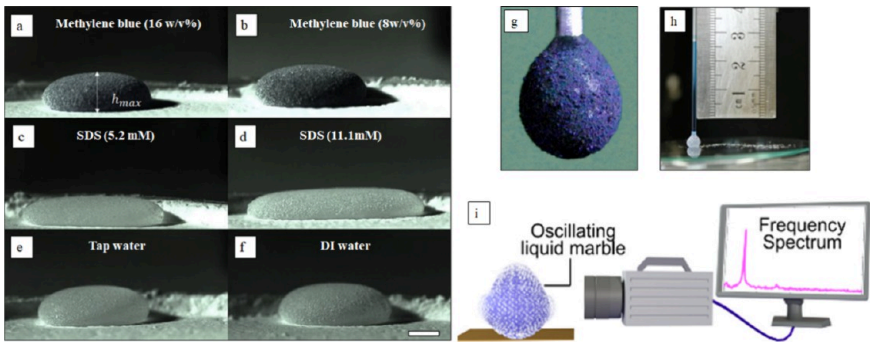

Figure 2. Various methods to measure effective surface tension. Maximum puddle height method for LMs. (a) Methylene blue (8 w/v %). (b) Methylene blue (16 w/v %). (c) SDS (below CMC). (d) SDS (above CMC). (e) Water and (f) tap water. The scale bar in (a−f) corresponds to 4 mm. Reprinted with permission from ref 9. Copyright 2022 Elsevier. (g) Pendant drop method used for surface tension measurement. Reprinted with permission from ref 55. Copyright 2013 Elsevier. (h) Capillary rise from a completely coated LM. Reprinted with permission from ref 56. Copyright 2011 American Chemical Society. (i) Oscillating sessile LM. Reprinted with permission from ref 57. Copyright 2021. Elsevier.

where r is the radius of the particle, γ_0 is the surface tension of the air−water interface, and θ is the CA of the particle straddling the interface. This energy of minimization of the interface is several times that of thermal energy kT causing irreversibility of adsorption. Particles that have a CA of 90° (partially hydrophobic) have the highest energy of attachment as they are partially wettable by both liquids and therefore bind better to the surface of droplets.[47] This does not hold true in the case of surfactants whose diameter is in the order of nanometers as thermal fluctuations allow easy desorption.

Understanding how solid particles stabilize an emulsion is dependent upon the wettability of each component (air, liquid) with the particle.[47,48] A phenomenon known as "transitional inversion" occurs where LMs are formed with 20% SiOH (highly hydrophobic) to that of foams with 40% SiOH (moderately hydrophobic) and stable aqueous dispersions with that of 60% SiOH (highly hydrophilic).[49] On the other hand, Whitby et al.[50] showed spontaneous LM formation by tuning the surface tension of core liquid by using ethanol−water mixtures. Liquids with intermediate surface tension consisting of a mixture of ethanol and water allowed the formation of LMs without any application of kinetic energy. "Dry water" was produced when there was a reduction in size from a macroscopic LM to a microscopic distribution of water droplets coated with hydrophobic silica particles.[31] Highly hydrophobic silica particles resulted in the formation of dry water with high mixing speeds and shear rates. A preference for high hydrophobicity of silica particles was identified to produce a stable dry water product which may otherwise transition to a mousse if the hydrophobicity was low.[51]

Next, particle−particle interactions adsorbed at such interfaces are discussed. Various capillary forces are present between particles depending on the particle size, shape, roughness, and their inherent wettability.[52] The concept of effective surface tension comes into play where particles used to coat a liquid droplet can either decrease, increase, or cause no changes to the original surface tension of the liquid.[53] The positive value of γ_{eff} corresponds to attractive forces between particles, and the negative value corresponds to repulsive forces.[54] Particles used to prepare LMs namely PVDF particles had attractive forces, repulsive for that of lycopodium and negligible for that of carbon black.[2]

$$\gamma_{eff} = \gamma_{int} + \gamma_{lv} \quad (2)$$

where γ_{eff} is the effective surface tension of liquid marble, γ_{lv} is the surface tension of bare air−liquid interface, and γ_{int} is the capillary force resulting from the interaction of particles. Several methods have been used to determine the effective surface tension of LM such as puddle height, analysis of marble shape, and analysis of eigen frequencies.[54]

A summary of various effective surface methods, their governing equations, and underlying mechanism is presented in Table 1. Additionally, their advantages and disadvantages are highlighted. The puddle height method is commonly used to measure the effective surface tension of LMs (Figure 2a−f). Measuring the maximum height of large puddle-sized LMs gives a clue about the magnitude of capillary forces involved.[9] Next, the pendant drop method showed the estimation of γ_{eff} depending upon the pathway of the experiment and rearrangement of particles[55] (Figure 2g). Here, γ_{eff} was also dependent on the volume of pendant drop, type of particle, and the number of particles on the surface. The volume of the drop dictated the interactions between particles with increased volume of the same drop, leading to effective surface tension values closer to that of water. On the other hand, decreasing the drop volume changed the LM characteristics to a quasi-solid. Thus, changing the volume of this coated drop showed pronounced hysteresis behavior. Particles like PVDF, SiO_2, and PE particles displayed strong interaction with a fast decrease in the overall effective surface tension with a decrease in volume. A gradual decrease in effective surface tension was seen for PVDF and lycopodium, while CB showed no change with or without changes in volume.[2] With an increase in the number of particles, a quasi-solid surface phase was obtained followed by buckling and ejection of particles.[58,59] When the volume is kept mid-dilution, clusters of particles separated by water clearing are observed. It should be taken into consideration that large and coarse particles give the drop a rough appearance, which leads to larger deviations in the Young−Laplace fitting parameter.[42] It is also possible that with dilution, particles from underlying multilayers are brought to the surface, thus changing the arrangement of particles which makes capillary interactions hard to visualize only with a macroscopic parameter.

The capillary rise method is another method used to estimate effective surface tension of LMs. The capillary rises are recorded from a flat-water surface and then a bare water droplet, which shows an additional capillary rise. LMs allow an extra height rise due to their coating (Figure 2h), which gives

https://doi.org/10.1021/acsomega.3c07657
ACS Omega 2024, 9, 12307−12330

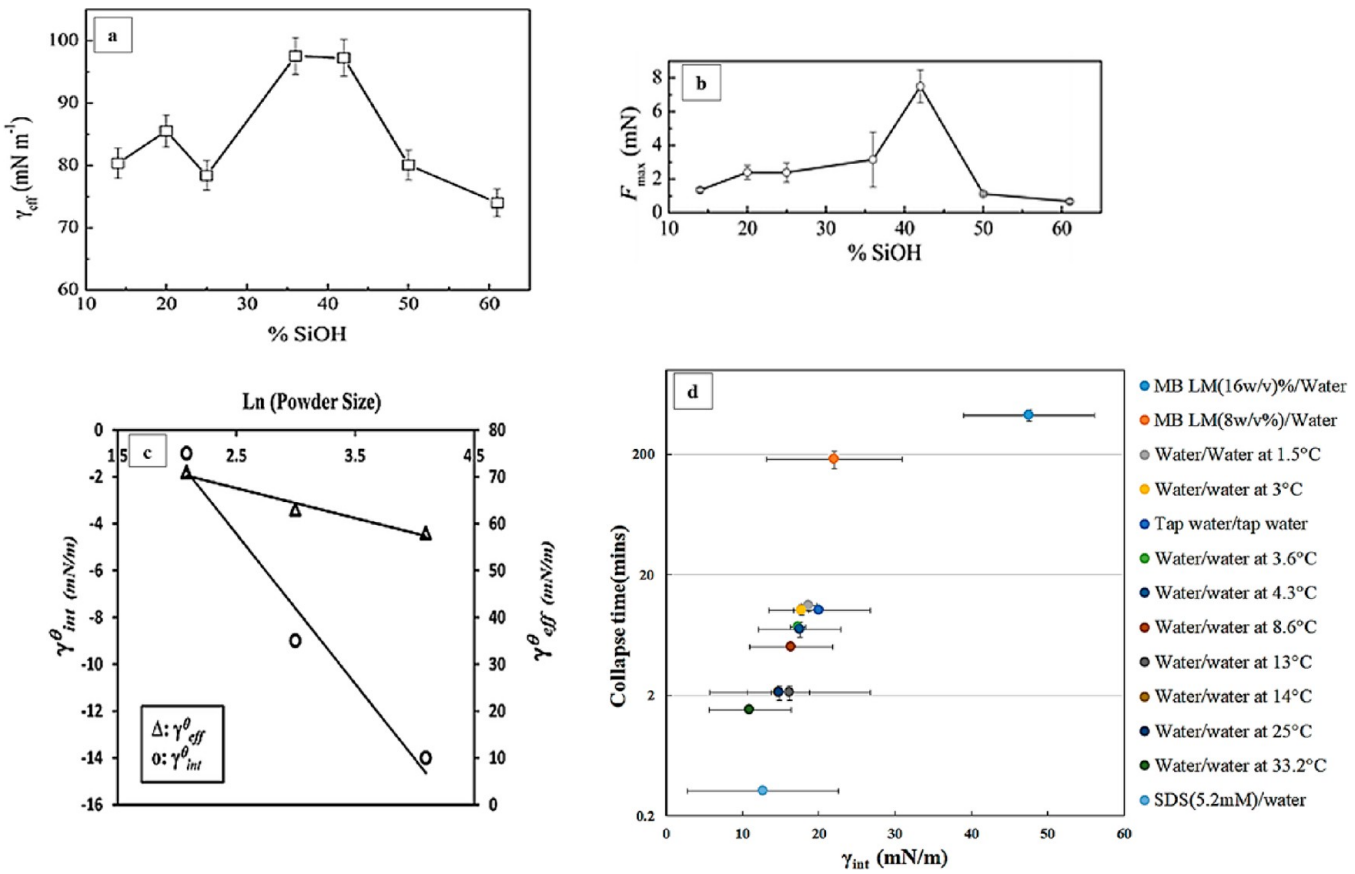

Figure 3. Correlation of stability of LMs with γ_{eff}. (a) Maximum force endured during squeezing of LMs (40% SiOH) matching that of (b) γ_{eff} values estimated for LMs. Reprinted with permission from authors of ref 67. Copyright 2013 Royal Society of Chemistry. (c) Change in γ_{int} of P-Zonyl TAN LMs with the logarithm of the size of these powders. Reprinted with permission from ref 66. Copyright 2013 Royal Science of Chemistry. (d) Dependence of collapse times of various floating LMs with γ_{int}. Reprinted with permission from ref 9. Copyright 2022 Elsevier.

insight into their effective surface tension.[56,60] Recently, Singha et al.[57,61] designed an oscillating apparatus to coat a liquid droplet uniformly and measure its γ_{eff} (Figure 2i). However, at high speeds, interfacial jamming occurred causing large deviation in the estimated values. Furthermore, for an elaborate discussion on effective surface tension of liquid marbles, these papers have been cited.[42,62,63]

To understand why γ_{eff} of an LM has increased or decreased, it is necessary to further probe capillary interactions between particles at the LM interface. Depending on the size of a particle, the capillary forces between a pair of particles occur as a result of the overlap of deformations by the meniscus formed by the particles.[52] When the particle size is larger than 5−10 μm, gravity-induced capillary forces come into force to decrease the overall energy popularly known as the "Cheerios effect".[64] The particles came together depending on the imbalance in hydrostatic pressure as well as the distance between them so as to constitute the horizontal force.[64] Vertical plates at a liquid−gas interface will attract if they have like menisci and otherwise repel.[65] This led to the fundamental idea of using surface tension to tailor the self-assembly of small-scale structures. If the diameter of the stabilizing particles is on the order of 1 μm or less, contact line undulation forces come into play. These forces occurred because the three-phase contact line was pinned to the heterogeneities of the particle surface, which induced an imbalance in the smoothly shaped meniscus.[72] This led to the formation of fractal-like structures of nanometric silica particles at the air−water interface increasing the stability of dry water.[51] Submicron silica particles of varied hydrophobicity at the air−liquid interface contributed to this force due to the pinning of the contact line because of roughness.[72] Additionally, these forces contribute to the exceptional stability of LMs undergoing compression and impact on a solid surface matching the estimation of effective surface tension of these LMs[67] (Figure 3a,b). The contact line for particles possessing 36% and 42% SiOH is longer since their θ_p are closer to 90° than other particles. Thus, intermediate hydrophobicity of particles led to highly robust LMs. Recently, Cengiz and Erbil[66] reported that the LMs made of larger size particles have a higher magnitude of repulsive forces and burst immediately, whereas LMs made of 8 μm particles are robust and remained floating for a longer time (Figure 3c) which was directly proportional to the γ_{int} values computed from γ_{eff}. The authors envisaged that large particles underwent repulsion and caused this floating LM to rupture early. On the other hand, LMs made of smaller particles had enhanced attraction due to contact line undulation. A similar approach was used by Ravi et al.[9] to investigate both particle−particle and particle−liquid interactions for various floating LMs, and their stability was directly dependent on capillary interaction (γ_{int}) (Figure 3d). Additionally, a critical threshold value of γ_{int} = 8 ± 5.6 mN/m was estimated to predict whether PTFE LMs can be prepared without rupture in the particle bed itself.

Coming to their application, the utilization of difference in γ_{eff} is used to drive liquid transport across two LMs made of

https://doi.org/10.1021/acsomega.3c07657
ACS Omega 2024, 9, 12307−12330

PVDF (70 mJ/m^2) and lycopodium (50 mJ/m^2) and was developed as a micropump model.[71] The liquid moved from PVDF LM to lycopodium LM until there was an equilibration of Laplace pressure (Figure 4a–d).

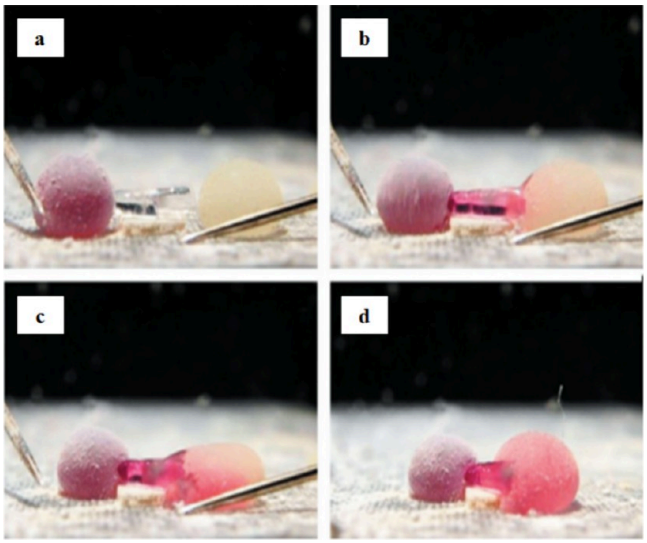

Figure 4. Fabrication of a functional micropump between LMs of varying γ_{eff}. (a) PVDF (red) and lycopodium-coated (yellow) LMs are separated. (b) Connection with a capillary tube. (c) Overflow from PVDF LM to lycopodium LM. (d) Lycopodium LM is swollen due to the flow, and a color change is observed. Reprinted with permission from ref 71. Copyright 2010 American Institute of Physics Publishing.

On another note, the effect of particle size to droplet size on LM formation is also discussed. Eshtiaghi and Hapgood[30] observed that LMs are formed when the droplet diameter is at least 25 times that of the particle diameter. This ratio was also observed in previously published works of LMs.[11,47,73−78] While considering this rule, the primary size of the particle must be used as most powders are aggregated.[38] However, there were exceptions to this rule. By using the electrostatic field for preparation of LMs, a ratio of as low as 1:12 was observed between those of droplets and particles.[79] The reason for this is still unexplained and has a possibility of formation of a novel class of LMs with layered or composite structures. Additionally, the failure of this rule was reported by Supakar et al.[80] during droplet impact on hydrophobized powders. This discrepancy was due to variation of hydrophobization techniques and aggregation of particles into rafts. In their case, a ratio of 6.8 was also reported for formation of LMs. Further, after increasing the particle size to 488 μm for droplet sizes of 1−3 mm, LMs could not be formed.[80]

2.2. The Wetting State. Before understanding how the state of wettability differs between LMs and drops on SH surfaces, the basics of these wetting states have been outlined. Figure 5a represents the change in surface free energy of drop at the three-phase contact line. The Wenzel wetting state[81] is given by

$$\cos\theta^* = r\cos\theta \tag{3}$$

where θ^* is the Wenzel CA, θ is the CA formed at the triple phase contact line, and r is the ratio between the actual to the apparent surface area of the substrate. An ideal Wenzel state constitutes a homogeneous wetting state with complete penetration into the roughness and a sticky hydrophobic situation[82] (Figure 5b). In the CB state,[83] the CA is an average between the value on air (180°) and that on the solid (θ) (Figure 5c). The ϕ_s is the fraction of the solid in contact with the liquid.

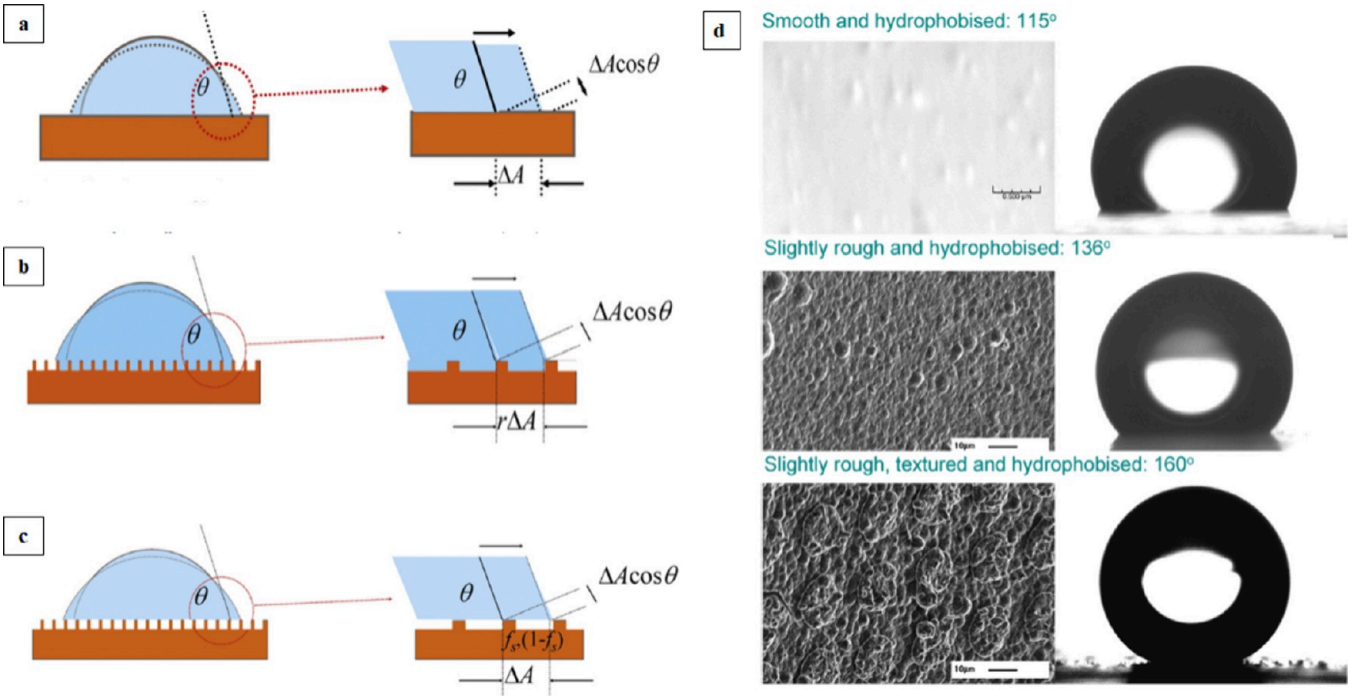

Figure 5. Wettability of a drop on various types of surfaces. (a) Change in surface energy of a drop on a surface. (b) Drop in a Wenzel state penetrating the roughness. (c) Drop in a CB state sitting on the top of the air pockets. (d) High CA as well as roughness is a prerequisite for superhydrophobicity. Reprinted with permission from ref 86. Copyright 2010. Elsevier.

https://doi.org/10.1021/acsomega.3c07657
ACS Omega 2024, 9, 12307−12330

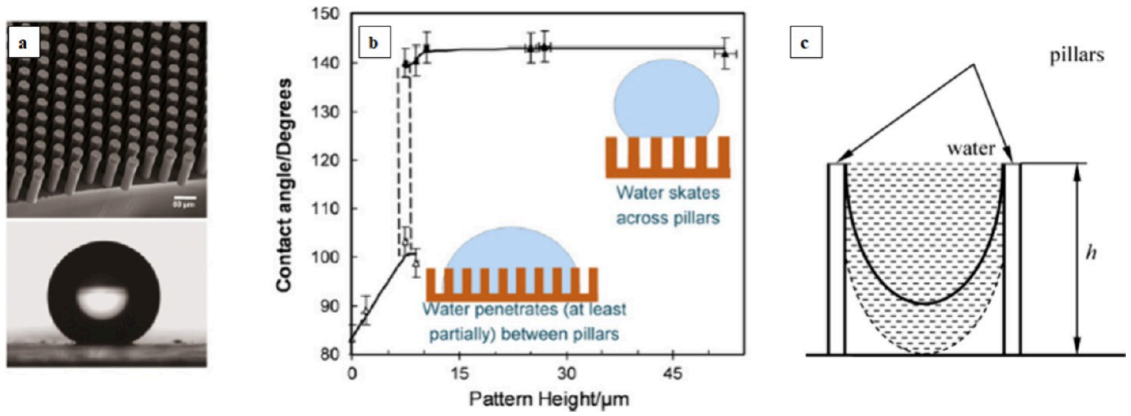

Figure 6. WTs as a function of surface topology of a SH surface. (a, b) Height of pillars increases the chances of a Cassie state. Reprinted with permission from ref 86. Copyright 2010 Elsevier. (c) Sagging transition of the drop between two pillars leads to the beginning of a WT. Reprinted with permission from ref 96. Copyright 2011 American Chemical Society.

$$\cos\theta^{CB} = -1 + \phi_s(1 + \cos\theta) \quad (4)$$

Air pockets were favored only if θ is larger than a critical CA θ_c.[84] The fractional area is a better measure of the hydrophobicity of the surface as it characterizes the surface features.[85,86] Though the Wenzel state constitutes a low energy, the drop may not always transition to it.[87] There is an energy barrier associated with these WTs like critical weight, pressure, or impact velocity of the drop.[88] The CB state and Wenzel state have an energy barrier between them, making one of them metastable and the other stable thus leading to "wetting transitions" (WTs).[89,90]

First, the wetting behavior of droplets on SH surfaces is identified. They are usually found in a nonwetting CB state depending on the topological architecture of the surface. A two-tier roughness allows better stability of the drop due to large capillary pressures (wetting energy barrier of the textured surface) thus making the drop more stable.[84,91] This demands a good pillar size as well as density in fabricated SH surfaces[92] (Figure 6a,b). Additionally, the shape of these pillars[93] influences the tortuosity of the triple phase contact line and thereby contributes to CA hysteresis depending on round-shaped pillars to star-shaped pillars. Innovative solutions such as combining smaller scale roughness at the base of the substrate with smooth pillars enhance CB state.[94,95] Probing these WTs in their microscopic nature showed that on surmounting a critical pressure, a sagging transition[96] of the contact line (Figure 6c) as well as a decrease in the thickness of air cushions[97] is observed.

This contact line is depinned and further depends on the two-tier roughness of the side walls of the material involved as well as the dimensions of the SH surfaces.[98] Other complex phenomena like stick−slip and formation of composite/mixed wetting states are also involved.[95] The challenge with creating SH surfaces involves going above a CA of 120°, which is not possible purely by chemical means, and roughness provides the most durable solution.[99] For example, lotus leaves consist of an intrinsically hydrophilic substance known as Carnauba wax having a CA of 74°, which is naturally superhydrophobic by surface texturing.[100] In addition to two-tier roughness, re-entrant structures inspired from nature (Springtail) have also been fabricated showing superior repellence to oils as well. These oleophobic structures consist of an oversized concave tip and a tapered pillar structure providing an upward force to the wetting of low surface tension liquids.[101] The study of WTs remains a test of robustness for fabricated SH surfaces[95] used for industrial purposes. Furthermore, sustaining the CB state during evaporation aids in the concentration of solutes and thereby interaction between them and the tops of pillars of a rough surface.[102] It is also possible to tune the movement of a drop either in a pinned state or a rolling state (reversible WTs) by electrostatic interactions.[103] Other applications utilize SH surfaces to enhance condensation heat transfer efficiency. The critical nucleation size of droplets is smaller than the order of roughness of SH surfaces, leading to flooding of the surface and breakdown of its superhydrophicity.[104]

Next, the wetting state in the case of LMs is explored. Here, the liquid drop is enwrapped with a shell composed of either hydrophobic[1] or aggregates of hydrophilic particles.[2] Even hydrophilic particles like carbon black[2] allow the preparation of LMs as these particles are nanometric and form aggregates which trap air and sit at the air−liquid interface of the drop. This is reminiscent of a fakir lying on a bed of nails.[99] The topological architecture of LMs constitutes a highly developed hierarchical roughness[84] trapping air pockets which allow enhanced lifetime, nonwetting and rolling ability of LMs not only on solid surfaces but also on liquid surfaces.[8] This can be observed by the ESEM images of the LM's shell showing clusters of particles separated by air pockets[105] (Figure 7a,b).

WTs in LMs constitute a loss of their nonwetting nature as LM remains stuck with liquid partially wicking into the powder bed. Decreasing the surface tension of the core liquid of LM[9] (Figure 7e) or decreasing hydrophobicity of particles[13] coating LM shell leads to an irreversible WT from the Cassie to Wenzel state. This is similar to drop WTs on SH surfaces, which in turn depend on the surface tension of bare droplet as well as the degree of roughness of this surface.[106] Bormashenko et al.[107] observed WTs on the addition of certain concentrations of ethanol into water LMs coated with PTFE, PVDF, and PE powders. LMs were stable in the CB state until a critical surface tension was reached which differed across these particles.

Like that of SH surfaces, WTs can also be used as a test of stability against surface tension changes of LM. Using surfactants like SDS at below and above CMC showed interesting phenomena during their transfer. While low CMC (5.2 mM) led to a change in the shape of LM from spherical to deformed shape, high CMC (8.3 mM) led to a rupture of LM

https://doi.org/10.1021/acsomega.3c07657
ACS Omega 2024, 9, 12307−12330

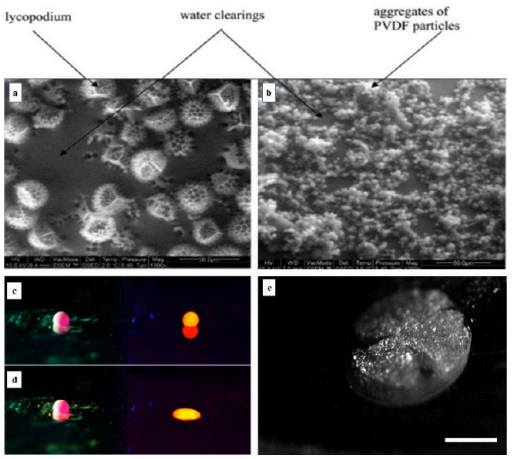

Figure 7. Topology of LM and their WTs. ESEM investigation of LM shell shows aggregates of particles separated by air clearings. (a) Lycopodium LM. Reprinted with permission from ref 35. Copyright 2011 Elsevier and (b) PVDF LM. Reprinted with permission from ref 108. Copyright 2009 Elsevier. Photograph of a 10 μL titanium coated LM (c) before UV irradiation and (d) after 30 min of irradiation leads to a tunable collapse of LM. Reprinted with permission from ref 109. Copyright 2014 American Chemical Society. (e) LMs made from SDS aqueous solutions (above CMC) collapse on the surface of spatula during the transfer from particle bed to liquid substrate. Reprinted with permission from ref 9. Copyright 2022 Elsevier.

outside of the powder bed (Figure 7e), thus reiterating the importance of a critical surface tension for the formation of LMs.[9] For SH surfaces, WT requires an energy input either with a change in either external force or wettability of the surface. Electrowetting of drop on SH-patterned surfaces led to irreversible wetting. In comparison, the surface coating of lycopodium protected the LM from wetting during the application of bias voltage. Here, the energy of detaching a hydrophobic grain from the liquid surface was higher and contributed to the LMs' stability.[110] Additionally, in section 3, the stability of LMs as well as drops on SH surfaces in terms of WTs are explained elaborately by using two such tests: evaporation and compression.

While WTs lead to loss of the properties of LMs, controlling them opens doors to their stimuli-responsive applications. Quick WTs in response to UV light led to the release of an inner payload in the case of hydrophobized TiO_2 coated LMs[109] (Figure 7c,d). Additionally, by utilizing WTs of particles coating LMs, the shell of LMs can be fused or ruptured, leading to on-demand manipulation. These LMs can also be coalesced to conduct microreactions[13] or release payload onto surrounding media. Furthermore, by keeping reagents in compartmentalized systems and only allowing their reaction by this WT can be made possible. Recently, WT of LMs was used to repair hydrophilic defects, and a sensor was fabricated anchoring a LM through a rose petal effect.[111,112] This opened avenues to intriguing applications of LMs to make durable and robust SH surfaces.

3. STABILITY ASPECTS OF LMs VS BARE DROPLETS ON SH SURFACES

3.1. Evaporation. For the evaporation of drops on SH surfaces, both constant contact angle (CCA) and constant contact radius (CCR) modes have been observed[113] (Figure 8a,b). Drops exhibit different modes depending on volume, nature of solid fraction,[114] as well as the hydrophobicity of the surface.[115] During evaporation of a drop on a patterned SH

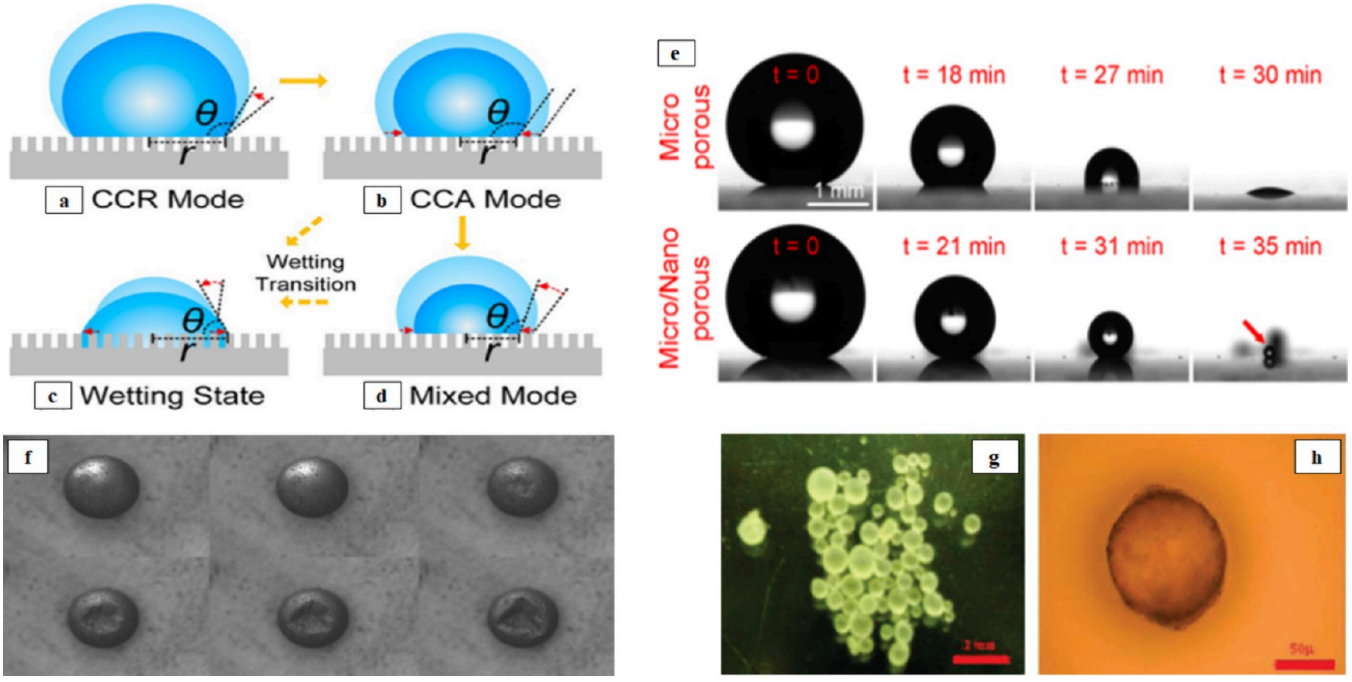

Figure 8. Behavior of droplet vs LM subjected to evaporation. Various modes of droplet on a surface during evaporation. (a) CCR, (b) CCA, (c) complete wetting, (d) mixture of wetting states. Reprinted with permission from ref 115. Copyright 2013 American Chemical Society. (e) High CB stability of drop at the micro-/nanoporous surface as compared to WT in the case of a microporous surface. Reprinted with permission from ref 124. Copyright 2014 American Chemical Society. (f) Stages of evaporation of a graphite LM showing the buckling of the top surface. Reprinted with permission from ref 11. Copyright 2009 American Chemical Society. (g) Optical imaging of a PDDA marble.[125] (h) Solid PDDA microspheres formed after evaporation of LM. Reprinted with permission from ref 125. Copyright 2010 American Chemical Society.

https://doi.org/10.1021/acsomega.3c07657
ACS Omega 2024, 9, 12307−12330

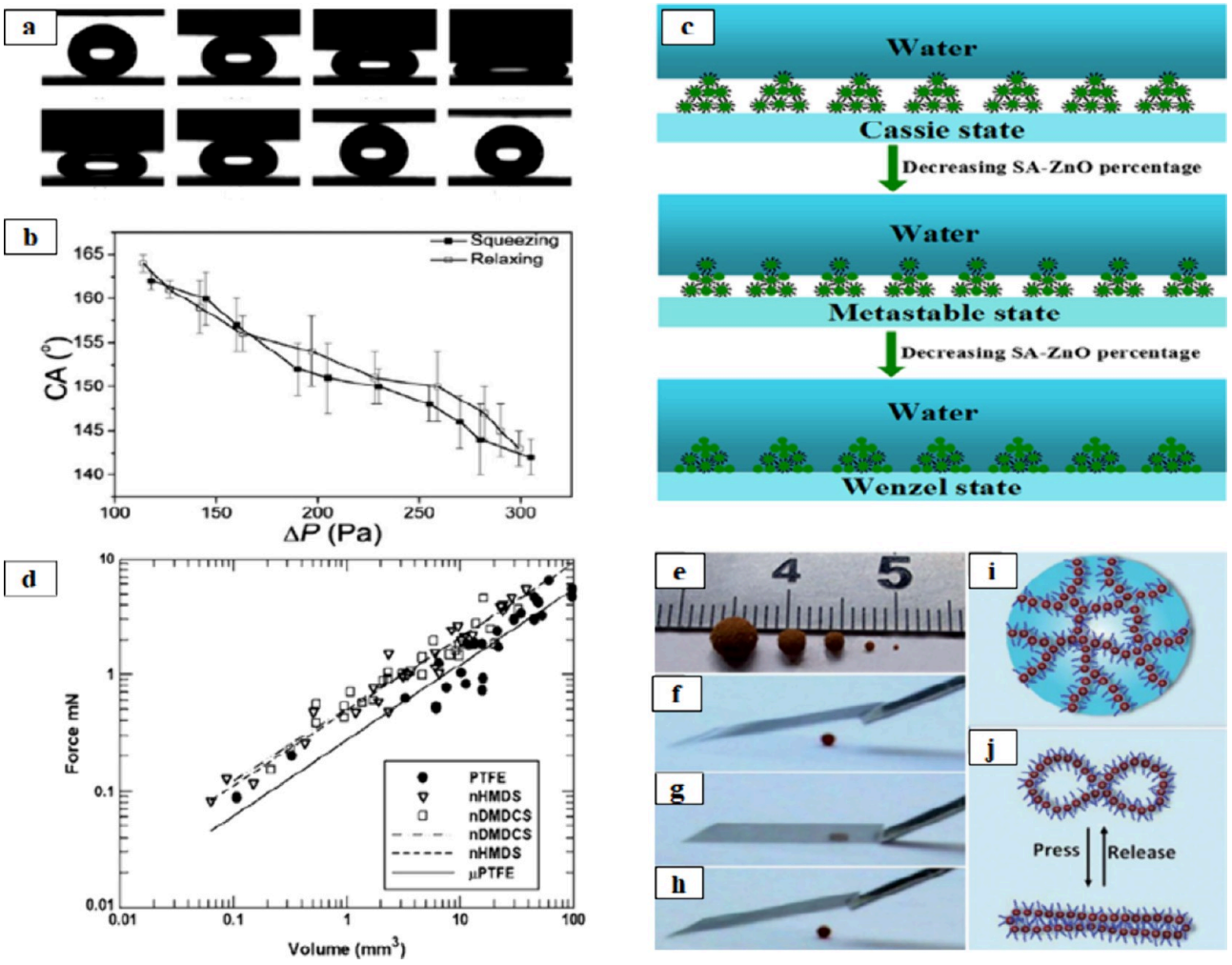

Figure 9. Testing the stability of drops on a SH surface and LM subjected to compression. (a) Sequential snapshots for a cycle of compression/relaxation. (b) Corresponding advancing angles and receding angles as a function of the imposed pressure show negligible hysteresis. Reprinted with permission from ref 135. Copyright 2010 Wiley. (c) WT by compression dependent on the percentage of Stearic acid-ZnO. Reprinted with permission from ref 137. Copyright 2014 American Chemical Society. (d) Force at rupture vs volume for PTFE, nHMDS, and nDMDCS marbles. Reprinted with permission from ref 74. Copyright 2008 American Institute of Physics Publishing. LMs of various volumes coated with compressible particles, (e–j) display of high compressibility. Reprinted with permission from ref 138. Copyright 2014 Royal Society of Chemistry.

surface, there is a decrease in the size of the drop, leading to higher Laplace pressures,[116] which increases penetration of the textures at certain points[97] (Figure 8e). At a particular CA or a base radius,[117] the drop is shown to suddenly wet the pillars by a sagging transition as mentioned previously.[118] In a wider perspective, evaporation of saline drops leads to fouling of surfaces due to the formation of pinned deposits/coffee-ring deposits.[119] Interestingly, conducting evaporation on a SLIPS led to a loss in anchoring of such deposits irrespective of the roughness of surfaces.[120]

A mixture of wetting states constituting CCA and CCR modes were also seen for LMs. LMs containing a binary mixture of water and ethanol showed a monotonously decreasing contact radius followed by buckling of the top surface.[121] PTFE LMs show an evaporation time of 26–60 min and are much more stable than bare droplets.[7] A similar type of behavior of almost twice the lifetime was reported for graphite LMs as compared to water droplets.[11] In both reports, diffusion-controlled evaporation and the addition of particles restrict the movement of water. Graphite LMs restricted evaporation more as compared to bare water drop as well as other LMs. The LM underwent a gradual decrease in CA followed by pinning onto the surface and buckling (Figure 8h). Bhosale et al.[74] estimated evaporation resistance by measuring the average rate of evaporation of LM vs that of bare drop. However, this parameter did not show changes with relative humidity. In contrast, Laborie et al.[122] reported that between LMs coated with monolayer vs bare droplets, LMs evaporated faster. This was attributed to the incompressibility effect of the LM structure. Otherwise, using NPs or a multilayered shell slowed down the evaporation rate. Above the Leidenfrost temperature, LM had similar characteristics with that of a water droplet. LMs are similar to that of Leidenfrost droplets in terms of thermal conductivity as well as the thickness of vapor layer and particle shells in LMs.[123] On pretreatment of PLA-LM known as "solvent vapor exposure" led to the formation of a thin film reducing the rate of evaporation.[126] Other routes to reduce evaporation include sulfur-stabilized LMs[127] which produce elongated surfaces and compensate the effect of the coating particles on evaporation rate. Nonetheless, the multilayer structure of particles contributed to the evaporation resistance and therefore longer lifetimes. Recently,

https://doi.org/10.1021/acsomega.3c07657
ACS Omega 2024, 9, 12307−12330

using a LM with a well-controlled monolayer or prerequisite knowledge of shell thickness led to the prediction of evaporation rates as compared to multilayered LMs.[6]

Next, the morphology of LMs resulting from interactions of particles is summarized. LMs formed with high surface NPs create stable shells because of an interconnected network of particles.[74] These were robust during evaporation as compared to the microsized material of the same particle. During evaporation, the surface topology of the SH surface dictates stability of a drop, while the nature of particle coating defines the stability of LMs. Recently, Gallo et al.[128] classified modes of evaporation by using a variety of particles as well as hydrophobicities. LMs showed three modes: constant surface area and buckling shown by moderately hydrophobic particles, particle ejection was seen with extremely hydrophobic particles with re-entrant structures, and in the last case, coarsening of the particle shell was observed due to enhanced interparticle interaction. This study also shed light on the behaviors of LMs in previous reports.[129] Also, the roughness of NPs used to make LM shell dictated its final structure after evaporation.[130] In the case of Fe_3O_4 NPs, dome-shaped LMs were obtained, whereas CNT-coated LMs produced near spherical shells. This further corroborates the importance of probing interparticle forces at both particle−liquid and particle−particle levels, which may lead to interesting assemblies after evaporation.

On another note, LMs could also be evaporated to form spherical hollow capsules, which can serve as storage and sensors.[125] Using a polyelectrolyte like PDDA allowed a gel-like phase transformation and formation of a robust solid capsule after evaporation (Figure 8f,g). Furthermore, LMs are used as precursors for hollow capsule formation with the use of special additives such as binders. Higher drying temperatures and nanosized particles lead to stable and hollow capsules.[75] Additionally, Roy et al.[131] used evaporation of LMs to pattern cavities and create roughness on surfaces by a soft-lithography technique. Studying a group of LMs at elevated temperatures helps design LMs for high throughput applications. Based on the arrangement of LMs as well as RH, these LMs could be designed as a minireactor for PCR as it operates on thermal recycling.[132] The same group of researchers[133] materialized this idea for using LMs as the PCR amplification setup. A high sensitivity of 28 ng/μL was obtained by visualizing fluorescence in LM and successfully synthesizing human fecal DNA. This has far-reaching implications for water quality monitoring. LMs are also utilized for the generation of healthy spheroids. It is still a challenge to make long-lasting LMs for 72 h for the cells to form spheroids. Adding a hydrogel compartment inside LM just by simple rolling leads to slowing down evaporation and also forming the adequate micro-environment for cells.[134]

3.2. Compression. In the case of compression of drop in SH surfaces, the topology again plays a crucial role due to the inherent capillary pressures generated within these textures. Drops on SH surfaces usually undergo a WT after a threshold pressure is reached during compression. Drops on SH surfaces with special architecture comprised of ribbed nanoneedles underwent a reversible WT (no hysteresis) upon compression due to nonpinning of contact lines as well as the formation of a metastable penetrating CB state[135] (Figure 9a,b). Surfaces with a hierarchical roughness on 2 or 3 levels showed exceptional stability to compressive load, the highest being reported at a Laplace pressure of 1450 Pa.[136] In addition to the effect of the surface geometry, the chemistry of the functional groups on the surface also plays a role. By tuning levels of hydrophobicity and hydrophilicity of ZnO groups on the surface, the drop can withstand pressures up to 640.9 Pa[137] (Figure 9c). Additionally, surfaces with double wettability have been engineered by using pH-dependent compounds, which lead to adhesion/sliding when pressed on the surface. Droplet interacting with the polymer chains gets pinned on the surface thus increasing the CA hysteresis.[139]

Similar to drops on SH surfaces, LMs exhibit a critical pressure which is dependent on their initial radius, uniformity of coverage, as well as their particle size. LMs coated with particles whose CA is closer to 90° allowed higher mechanical robustness.[140] In addition, NPs on account of forming a network of interconnected particles underwent higher compression and thus were more stable, which was also reported during evaporation previously[74] (Figure 9j). Further, hydrophobically modified magnetic particles gave rise to highly compressible LMs because of mutual entanglement of their chain-like structures[138] (Figure 9d−i). LMs made of biomimetic cellulose acetate fibrous mats handled 10 times the compressive deformation as compared to normal particle-coated LMs (12.3 mN as compared to 1−2 mN) due to high tensile capacity of the fibrous mats.[141]

The ductility of LMs is dependent on both particle composition as well as the volume of LMs.[142] Coating particles such as lycopodium form well-distributed rafts due to increased interparticle attractions as compared to PTFE. In contrast to previous reports of using nanometric-sized particles, Liu et al.[143] observed that larger particles packing into a hexagonally closed arrangement led to an increased magnitude of gravity-induced capillary interactions.[64] Using larger particles to coat LMs led to better resistance against compression up to 82 ± 5 Pa even if blended in large quantities. Recently, Rane et al.[144] reported the compression of LMs coated with spherical glass particles and coarse PTFE particles. Spherical particles and high surface tension of liquids[145] performed better under compression. Also, LMs made of various shaped particles such as spherical and rods of $CaCO_3$ particles showed varied compression behaviors.[146] By applying compression−decompression cycles, spherical particles arranged better at the air−water interface as compared to rod-shaped particles which formed a 3D network thus resisting rearrangement. This could also be related to the effective surface tension of spherical particles which was higher than that of rod-shaped particles. Huang et al.[147] went one step forward by testing the compression of LMs on substrates of different wettabilities. Monolayer jammed NP (~20 nm) shelled LMs broke easily during compression; however, increasing the hydrophobicity of the compression plates allowed better stability of LMs as well as their transport. Recently, sulfur-stabilized LMs consisting of an inner hydrogel layer that were stable up to 53% of relative compression were reported.[127]

Pressure-sensitive adhesives (PSAs) are challenging to deliver in confined spaces due to their handling. Delivery in the form of LMs serves a dual purpose allowing PSAs to behave like a dry powder as well as undergo easy transport by rolling.[148] Coating this special polymer in a hard NP shell allows the use of two processes, evaporation and application of compression, leading to an outflow of this soft polymer. This exhibited their innovative encapsulation and on-demand release mechanism by compression. Recently, LMs allowed the *in situ* synthesis of polyperoxides due to the porous shell of

https://doi.org/10.1021/acsomega.3c07657
ACS Omega 2024, 9, 12307−12330

LM followed by their stimulated release by compression as well as controllable adhesive strength.[149] Further, color change with response to compression (mechanochromic response) has been shown with LMs prepared with cholesteric solutions, leading to their self-assembly which were inherently color-dependent.[150]

4. COMPARISON OF DROP DYNAMICS ON GRANULAR MEDIA VIS-À-VIS HARD SURFACES

4.1. Dimensionless Numbers and Maximum Spread.

A droplet of initial diameter D_o impacting a flat or granular surface achieves a maximum spread D_m depending upon a variety of parameters.[151] The spherical nature of the initial droplet is transformed into an oblate disc shape depending on impact velocity, the roughness of SH surface/packing fraction of the granular bed, and the physicochemical properties of the fluid used. The kinetic energy of this droplet before impact is then used to create a new surface during maximum spread. The maximum spread ratio $\beta_{max} = D_m/D_o$ is an indicator of the various parameters influencing the drop impact.[33] During spreading, other dissipations such as internal circulations[152] and viscous dissipations[153] also occur. To characterize β_{max}, dimensionless numbers such as Weber number (We), Reynolds number (Re), Bond number (Bo), Ohnesorge number (Oh), and Capillary number (Ca) were used. The formulas for these numbers contain ρ, which is the density of the droplet, g is the acceleration due to gravity, and V is the impact velocity. γ and μ represent the physicochemical properties of the fluid namely, surface tension and viscosity.

$$\mathrm{We} = \rho D_o V^2/\gamma \tag{5}$$

$$\mathrm{Re} = \rho D_o V/\mu \tag{6}$$

$$Bo = \rho g D_o^2/\gamma \tag{7}$$

$$Oh = \sqrt{We}/\mathrm{Re} \tag{8}$$

$$Ca = \mu V/\gamma \tag{9}$$

First, the We number is a ratio of inertial force to that of surface tension and shows the extent of drop deformation.[30] Next, the Re number is a ratio of inertia to that of viscous forces and indicates the influence of viscosity.[30] $\beta_{max} \approx We^{1/2}$ scaling was observed for drop impact on flat surfaces assuming that there is pure transfer of kinetic energy to surface energy.[154] Considering the shape of the drop experiencing an imposed acceleration γ is of the order ${V^2}_0/D_0$, the spreading of the drop followed a scaling of $We^{1/4}$. Further, increasing viscosity of liquid and high impact velocities led to $\beta_{max} \approx Re^{1/5}$. Coming to internal circulations, Wildeman et al.[152] reported the occurrence of recirculation eddies during droplet spreading for $We > 15$ and $Oh \ll 1$. This has also been shown in the work of Clanet et al.,[154] where such eddies could be visualized in a balloon undergoing sudden acceleration. This contributes to a half energy loss in the energy budget of a droplet undergoing impact on both flat as well as granular surfaces. These eddies can occur when the bulk of the droplet moves from the lamella to the rim. This has been visualized by particle-tracking in the work of Lin et al.[155] where a circular flow occurred in the droplet rim which varied with impact velocity as well as viscosity. Further, this half-energy loss has been shown to be the lower limit of energy loss for a free-slip surface as compared to that of a no-slip surface.[152] While energy balance models have been continuously evolved for the drop impact on flat surfaces, such models are still in their infancy for those of drop impact on granular surfaces.[80,156] A broad crossover regime between $We^{1/2}$ (capillary regime) and $Re^{1/5}$ (viscous regime) was deemed optimum and allowed to explain the scaling of data.[157] We and Re change as a result of the physiochemical properties of liquid as well as the roughness of the surface.[158] β_{max} increased with increasing We and Re; however, identifying a critical We number failed when rough surfaces were introduced. A scaling of the We number for the different types of surfaces used ranged from 0.2 to 0.3; however, there was a lack of precision.[159] Recently, We number scaling using ethanol, glycerol, and water was estimated. However, only water seemed to fit the $We^{1/4}$ scaling, whereas glycerol exhibited $Re^{1/5}$ scaling.[160] On another note, microdroplet impact falls in between that of capillary and viscous regime.[161] For a given We, the microdroplet spreading is lower than that for mm-sized droplets due to viscous effects.

Next, the maximum spread behavior in the case of drop impact on granular surfaces was discussed. $We > 1000$ successfully predicts that the drop will shatter after impact on the hydrophobic powder bed.[30] A We number scaling of 0.3 was obtained for smaller drops, and the scaling failed for larger drops impacting on compacted glass beads.[80] We number scaling of 1/5 was estimated considering the cushioning effect evident in powder surfaces.[162] For hydrophilic granular beds, the liquid mixing with grains affects the drop spreading characteristics.[163] The We scaling here ranged from 1/4 and 1/10. Though the 1/4 scaling matched previous literature reports with a drop undergoing sudden acceleration, it was not the case for 1/10 scaling. This peculiar scaling also reflected the viscous dissipation, and this was true for drop spreading on large hydrophilic grains.[164] We and Re scaling of hard surfaces with those of granular surfaces were matched, and this scaling approach failed.[165] The packing fraction of the granular bed also played a major role in the energy dissipation, and it is significant when considering the energy balance as well as the splashing threshold which is discussed later.

Next, Bo is a ratio of gravitational forces to that of surface tension forces. It characterizes the shape of the drop and gives an idea of whether the drop will remain spherical with a threshold value of 1. This value was applicable for checking the sphericity of drops on both flat and granular surfaces. For $Bo > 1$, drops are larger than the capillary length so that different shapes are expected at maximum deformation.

The Oh number relates the viscous forces to inertial and surface tension forces.[30] Providing an Oh number threshold also gives an indication of whether droplet will deposit, which is useful for pesticide spray applications.[166] However, this number has been seldom used as their limits were not applicable to all drop impact-granular bed systems. Next, the Ca number allows for studying the combined effects of surface tension and viscosity. This number helps to study the retraction phenomena, especially in dynamic CA studies. Oh and Ca numbers are further described in the case of the retraction phenomena of droplet.

It is evident that scaling with dimensionless numbers provides an incomplete picture of maximum spread. Regarding coating of a drop in case of drop impact on granular beds, the relationship of dimensionless groups with coverage is still missing and requires further investigation.[34]

4.2. Retraction, Jetting, and Rebound Behavior.

After the spreading of a drop on the surface, a droplet undergoes a

https://doi.org/10.1021/acsomega.3c07657
ACS Omega 2024, 9, 12307−12330

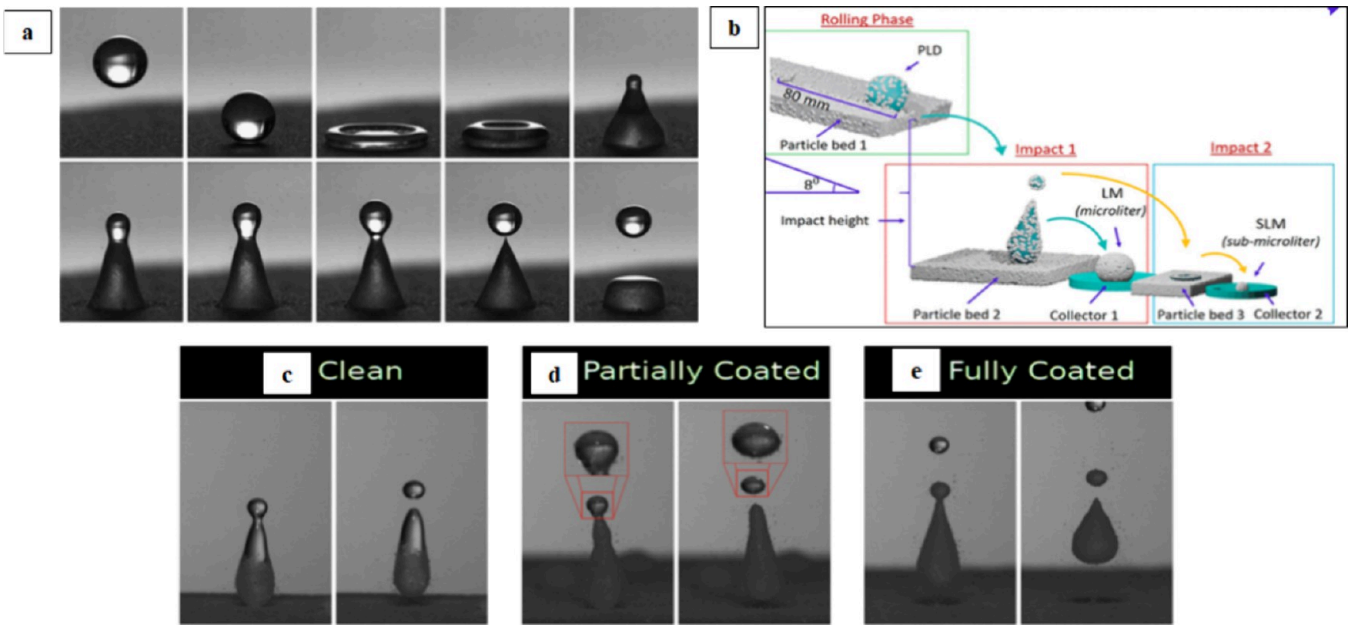

Figure 10. Characteristics of jetting and pinch-off. (a) Drop undergoing a partial pinning and jetting on granular bed. Reprinted with permission from ref 162. Copyright 2010 Elsevier. (b) Production of submicron LMs by utilizing jetting and formation of satellite drops. Reprinted with permission from ref 28. Copyright 2022 American Chemical Society. Coating of satellite drops by jamming (c) uncoated/clean, (d) partially coated, (e) fully coated. Reprinted with permission from ref 187. Copyright 2021 American Physical Society.

dynamic process of retraction followed by rebound. The retraction rate of drops on solid surfaces remains constant and is not dependent on the impact velocity. Similar to the drop spreading phenomenon on flat surfaces, drop retraction can occur in a viscous and an inertial regime.[167] For an elaborate discussion on drop receding dynamics, this work[168] is cited. The value of receding CA determines whether a drop will rebound off a SH surface.[169] Static CA does not affect the dynamic CA until the maximum spreading is reached. The dynamic CA falls as the *Ca* number increases considering the velocity of the contact line. At lower *We* numbers, the effect of surface tension on the retracting lamella is higher, leading to lower *Ca* numbers. Trapping of the air bubble and a large CA of 180° are valid for the spreading phase but is lost during the retraction due to its dynamical aspects.[170] Recently, a "plateau contact angle" (dynamic advancing CA) was identified and controlled by the competition between surface tension and viscosity.[171] The *Oh* number versus this angle provided an indication that at high *Oh* numbers, the variation of this angle reduces.

The prevention of retraction of droplet impacting on hydrophobic leaf surfaces is a prerequisite for ideal pesticide formulations as their leaching into groundwater can be detrimental to the environment.[172,173] Surfactants are commonly used to arrest drops in their retraction phase itself. However, the diffusion of the surfactant molecules to the new interface created during spreading depends on the dynamic surface tension of the surfactant and thus influences its spreading capabilities.[174] On the other hand, rebound off fabricated nonwetting fabrics[175] and heat exchanger tubes[176,177] is crucial in controlling their fouling.

After the retraction of the droplet, a prolate jet shape is achieved with tapering of its edge leading to pinch-off at the tip. Entrapment of an air cavity during retraction of the drop leads to increased velocity at the tip followed by jetting and ejection of satellite droplets.[166,178] Binders such as carboxy methyl cellulose led to the arresting of jetting by the formation of a thin ligament attached to the bulk of the droplet. Therefore, the drop cannot bounce and dissipates its excess energy stuck on the surface. Next, the drop may undergo rebound on the surface due to its excess energy. This is the remainder of the surface energy left in the drop after viscous dissipations and internal circulations during spreading.[33,179] The ability to rebound depends on the wettability of the surface and the physicochemical properties of this fluid.[180] If the viscous dissipation is too large during drop retraction, such drops will undergo weaker oscillations. Further, low surface tensions of liquid can possess higher spreading capability thus leading to deposition. The roughness of the flat surface also plays a key role in rebound. A coexistence of rebound and pinned states can be visualized depending upon the roughness and velocity of impact. This again crosses the foray into the stability of the CB state depending on the periodicity and length scale of the roughness of the flat surface as discussed earlier.[181] In earlier reports, small amounts of polymer arrested the rebound due to elongational viscosity associated with polymers.[182] Drops containing polyacrylamide anchor themselves to the substrate and lead to partial pinning and loss of rebound.[183]

Retraction remains to be explored in detail for powder surfaces with respect to its dynamic aspects. At low velocities, retraction of droplet on a granular bed was reported by Whitby et al.[184] The spreading is negligible, while the retraction is dominant as the drop behaves like a spring due to increased capillary forces. The droplet rotates on the surface collecting powder on the underside followed by bouncing. This drop was also seen to roll away from its original location due to the heterogeneities of the powder bed. On another note, retraction of a highly particle-loaded LM on the SH surface was compared with that of a drop. The particles of the LM interact with the underlying SH surface causing perturbations and additional energy dissipations due to the development of a

https://doi.org/10.1021/acsomega.3c07657
ACS Omega 2024, 9, 12307−12330

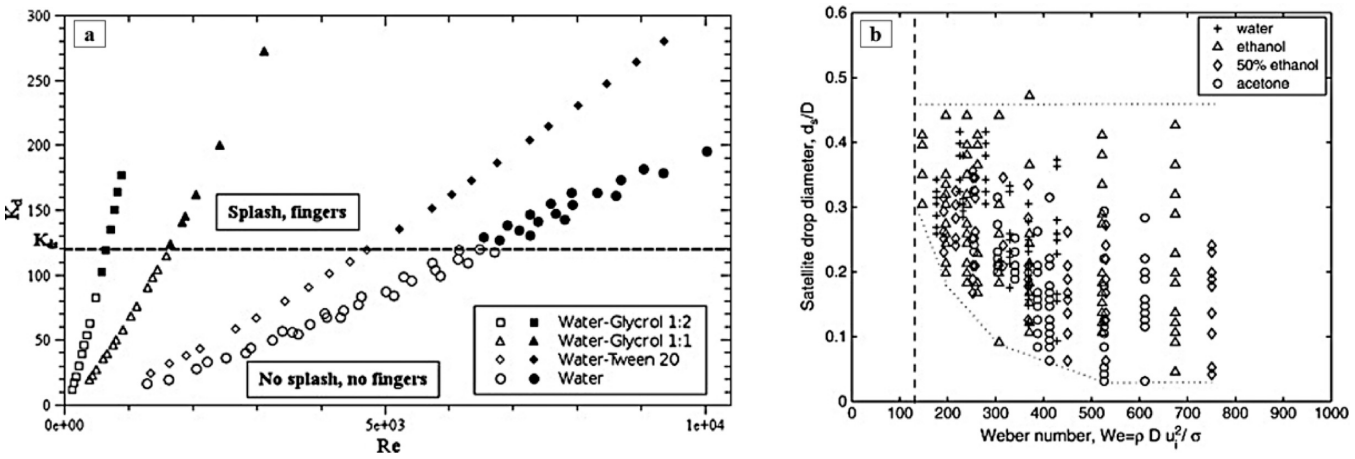

Figure 11. Splashing of drops in the case of droplet impact on granular beds. (a) *K* as a function of the *Re* number. Reprinted with permission from ref 165. Copyright 2012 Elsevier. (b) Satellite drop diameters plotted against the *We* number for liquids exhibiting a wide range of diameters. Reprinted with permission from ref 162. Copyright 2010 Elsevier.

"roughness-based wettability contrast".[185] On the contrary, droplet impacting a SH surface would quickly retract due to high CAs and undergo jetting based on the *We* number. For droplet impact on powder surfaces, jetting depends upon the viscosity of droplet and the packing fraction of the granular bed.[162] Decreasing the packing fraction of the bed leads to a change in the thickness of the jet along its length.[186] The satellite droplets formed during jetting are analyzed with respect to drop impact on granular beds. At *We* numbers of 55, particle-laden drops of controllable submicron range (200 nL to 18 μL) can be generated by jetting[28] (Figure 10b). These submicron LMs presented higher sensing and stability as compared to their microlitre counterparts.[28] Pritchard et al.[187] tuned the coating of satellite drops to clean, partially coated, and fully coated based on the coating of the jet itself (Figure 10c–e). Also, the "squashing" phenomena of highly coated LMs was captured where the satellite drop merges into the jammed jet structure.[187] On the contrary, jetting could be suppressed by higher mass loading of LMs at *We* (57–92) numbers resulting in interesting flower-shaped patterns.[185] This special feature occurs at lower *We* numbers as compared to the impact of bare droplets on SH surfaces.

Next, the rebound phenomenon of droplet after retraction on granular beds is reviewed. This is also dependent on the viscosity of the droplet leading to reduced bouncing as that of SH surfaces.[188] LMs are heavier than drops and undergo damped oscillations due to the entrainment of powder during each spreading-rebound cycle. A mass increase of LMs between 5% and 45% of the original mass of the droplet was approximated.[162] By increasing the packing fraction of the powder bed, the apparent CA can be increased, leading to enhanced rebound behavior. At low packing fractions, energy is dissipated more into the formation of craters and ejecta thus leading to negligible bouncing.[162] Here, the packing fraction of the powder beds has similar roles to the roughness of the flat SH surface.

Bouncing to pinning transition also occurs in the case of the drop impact on powder beds.[162] During retraction, a part of the drop remains pinned onto the heterogeneities of the powder surface due to partial liquid penetration (Figure 10a).

The consequences of the rebound phenomena are discussed with respect to the maintenance of the soil environment. Rebound and fragmentation of raindrops could prove deleterious as it increases the chances of soil erosion.[189,190] Soil contains a mixture of hydrophobic and hydrophilic components influencing rebound at low velocities of drop and fragmentation at higher velocities. Absorption of hydrophilic components into drop leads to lower fragmentation due to capillary forces between these particles.[191] In addition, the characteristics of soil are largely affected by wildfires thus changing their inherent wettability characteristics. The formation of coated droplets or LMs on fine sand led to increased erosion, and their effect on inclined surfaces was further magnified due to their rolling behavior.[192]

4.3. Splashing and Outcome of the Drop. A variety of splashing behaviors are observed for drop impact on flat surfaces such as deposition, corona splash, and receding breakup.[193] The final outcome of drop impact on solid surfaces can be broadly classified into deposition and splashing which is further divided into the corona and prompt splash.[194] Deposition is characterized by a spreading lamella that does not have ejection/breakup of the liquid sheet. Prompt splash was dependent on the degree of roughness of the surface, while corona splash depended on the pressure of the surrounding gas.[195] Roughness threshold in the case of prompt splash plays a significant role in understanding blood stain patterns in forensics.[196] Also, the presence and composition of surrounding gas can affect the splashing of drops.[197,198] Next, by tuning the surface geometry, the direction of splashing can be controlled, thereby tailoring the number of ejected drops.[199]

We and *Re* numbers could not adequately describe the boundary between splashing and nonsplashing.[200] A scaling of $Oh{\cdot}Re^{0.89} = 0.85$ was empirically derived from the graph of *Oh* vs *Re* number. This was further simplified to $Ca^{1/2}$ by considering $Re = 0.5$. High $Re > 4000$ showed the occurrence of prompt splashes, whereas low *Re* was captured as corona splash.[194] Early reports demonstrated that the splashing parameter $K = We^{1/2}\ Re^{1/4}$ can be indirectly described by the natural free oscillation of the drop, and the number of fingers are dependent on the inertial-viscous interaction of the drop-hard surface.[201] *K* was tested to predict the number of fingers formed during the high-velocity impact of molten metal droplets.[202] Assuming Rayleigh-Taylor instability, the number of waves formed around the rim of the drop increased with the increased velocity of the drop. In this case, $K > 57.7$ led to splashing. For nanofiber mats, a high value of $K = 87$ was

https://doi.org/10.1021/acsomega.3c07657
ACS Omega 2024, 9, 12307−12330

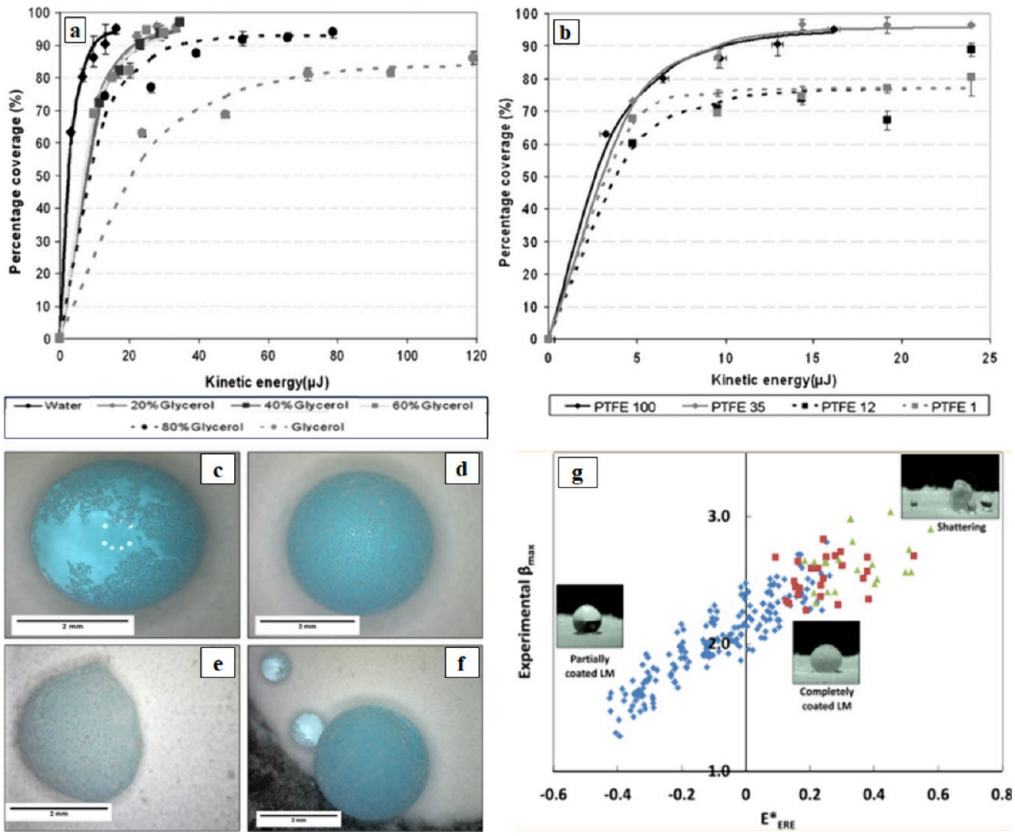

Figure 12. Magnitude of particle coverage of droplet. (a) Effect of viscosity. (b) Effect of particle size. Reprinted with permission from ref 34. Copyright 2009 Elsevier. Outcomes of drop impact on hydrophobic particle bed forming LMs, (c) partially coated, (d) completely coated, (e) deformed, (f) shattering of drop to yield daughter droplets. (g) Experimental β_{max} vs excess energy predicts coating of LM. Reprinted with permission from ref 33. Copyright 2019 American Chemical Society.

obtained because of suppression of advancing splash.[203] The complex nanostructure as well as the porosity of these mats led to pinning and adsorption events. Recently, Quetzeri-Santiago et al.[204] reported that *Ca* numbers and *K* cannot differentiate between splashing and nonsplashing behavior when a variety of liquids and surfaces were tested. Understanding how the dynamic advancing CA changes during splashing and estimation of the "splashing ratio" was a better indicator.[204]

In the case of increased viscosity of the droplet, the velocity for splash transition also increases.[205] However, this change does not occur in a monotonous fashion as described in the work of Palacios et al.[206] At high and low *Re* numbers, viscosity promotes splashing, whereas at a critical $Re < 1000$, splashing is suppressed. This contradictory observation is due to lack of in-depth measurement of lamella behavior at various *Re* numbers. Droplets with viscosities of 5cst promote splashing, whereas droplets of viscosity greater than this value suppress splashing behavior. This can be explored in depth by a profound understanding of lamella dynamics and its thickness.[207]

Coming to drop impact on granular surfaces, Nefzaoui and Skuryts[165] showed that the granular medium ends up delaying the splashing behavior of droplets. The number of fingers could not be estimated correctly due to reasons such as the coalescence of drops, merging of fingers and inability to form fingers. For granular beds, $K = 120$ was obtained which was higher as compared to that of flat surfaces due to the damping effect of the granular bed[165] (Figure 11a). Changing the packing fraction of the powder bed also changes the number of satellite drops as well as their diameter. Further, liquids of low surface tension had a higher propensity to shatter across *We* numbers, leading to a wider size range of satellite droplets (Figure 11b). At the same velocity, a powder bed roughened by artificial scraping generates 5 drops in the range of 620−760 μm. Without this modification, 25 such satellite drops were formed in the range of 160−740 μm. The size and number range of satellite droplets have implications for the formation of granule nuclei in the pharmaceutical industry.[162] Also, the number of drops decreases with increasing surface tension and/or viscosity for a given impact velocity that of drop impact on flat surfaces. While drop splashing on rough surfaces could be classified into many outputs, it was hard to define splashing on granular surfaces in this regard due to formation of craters and ejecta. Recently, the drop impact on a monolayer of particles showed corona splashing due to the high mobility of particles and formation of packed particle layer during the formation of rim.[208]

After looking at how splashing differs in granular surfaces, varied phenomena of droplets undergoing coating is highlighted (Figure 12c−f). The magnitude of coating of LM (partially/completely coated) is dependent on parameters such as viscosity, impact velocity, and particle size[34] (Figure 12a−b). At intermediate velocities, high surface tensions, and low viscosity, completely coated LMs were obtained.[34] Further, an energy balance model based on β_{max} was formulated to determine the complete coating of LMs.[33] $\beta_{max} > 2$ and positive excess energy E^*_{ERE} led to the formation of completely coated LMs (Figure 12g). However, this was qualitative in

https://doi.org/10.1021/acsomega.3c07657
ACS Omega 2024, 9, 12307−12330

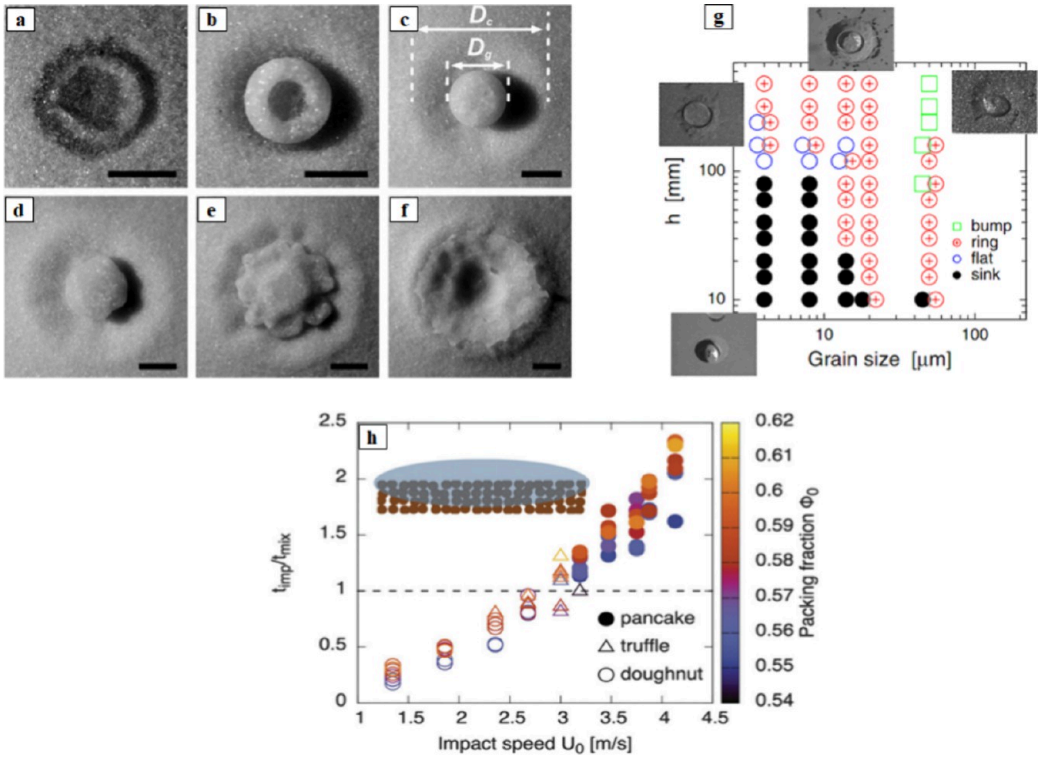

Figure 13. (a–f) Morphology of crater residues depending on the impact velocity transitioning from ring to a jammed shape. Reprinted with permission from ref 213. Copyright 2015 Proceedings of the National Academy of Sciences. (g) Phase diagram of various crater shapes by varying grain size and height. Reprinted by permission from ref 212. Copyright 2010 American Physical Society. (h) Effect of packing fraction. Reprinted with permission from authors of ref 219. Copyright 2015 Royal Society of Chemistry.

nature and could not delineate the occurrence of completely coated LMs and shattering.

Additionally, the question of formation of uniformly coated LMs with a set of known multilayers through this route remains open. Modulating the magnitude of LM coating can open doors to potential applications. For example, partially coated LMs have been used for asymmetrical interfacial crystallization of NaCl,[209] completely coated LMs are being used as immersion microreactors,[210] and puddles also have been used to create compartments for electrode-assisted catalysis.[211]

4.4. Cratering in Granular Media and the Formation of Ejecta. The crater dissipation plays a significant role in understanding the drop impact on granular surfaces and helps in the correct prediction of β_{max} during the formulation of energy balance models. The diameter, depth, and morphology of residues can be used to characterize a crater.

The density ratio allows predicting drop deformation as compared to other parameters as spreading is caused by the difference between the density of the bulk granular layer ρ_g and that of the water drop ρ_w, which directly reflects the influence of the packing fraction of the granular bed. Here, R is the crater radius, and R_w is the initial diameter of the droplet.[188,212]

$$\frac{R}{R_W} = \frac{\rho_g}{\rho_w} \cdot We^{1/4} \tag{10}$$

Similar to dimensionless scaling of maximum radius with the We number, Zhao et al.[213] developed a scaling of crater diameter with that of crater energy dissipation ($D_c \approx E^{1/4}$). However, this may be applicable only for low-speed solid sphere impact cratering as reported previously.[214] This phenomenon follows Schmidt–Holsapple (S–H) scaling,[215] which is applicable in asteroid impacts, though there is an enormous length scale as well as energy difference to that of drop impaction on granular beds. This large energy partitioning occurs in the case of drop impact on granular beds where the kinetic energy of the drop is dissipated by viscous and surface energies like that of asteroid impacts where the energy is dissipated in the form of shock waves. Further, an intriguing analogy was developed between asteroid impacts and droplet impacts showing a similar aspect ratio $\alpha = d_c/D_c$ of 0.2 where d_c is the depth of the crater and D_c is the diameter of the crater, respectively.[213]

$$D_c \approx (\rho g)^{-0.17} D^{0.32} E^{0.17} \tag{11}$$

where U and ρ are the impact velocity and density of the projectile. Surprisingly, D_c weakly depends on liquid properties such as density, viscosity, and surface tension.

On the other hand, understanding crater depth is a challenge because of multiple fluid-granular interactions.[163] Recently, drop deformation leading to high energy partitioning was used to explain why crater diameters for drop intruders are higher as compared to that of solid sphere intruders.[216] However, the same does not hold true for crater depth. Crater depth is dependent on the remaining energy of the drop after spreading and ejecta formation. Hence, crater depth is greater in the case of solid sphere intruders as compared to droplets.[216] Further, the deformation of the intruder could be tuned by using hydrogel spheres of various stiffness impacting on target granular beds. The decreased stiffness of these hydrogel spheres led to greater deformation and thus greater crater

https://doi.org/10.1021/acsomega.3c07657
ACS Omega 2024, 9, 12307–12330

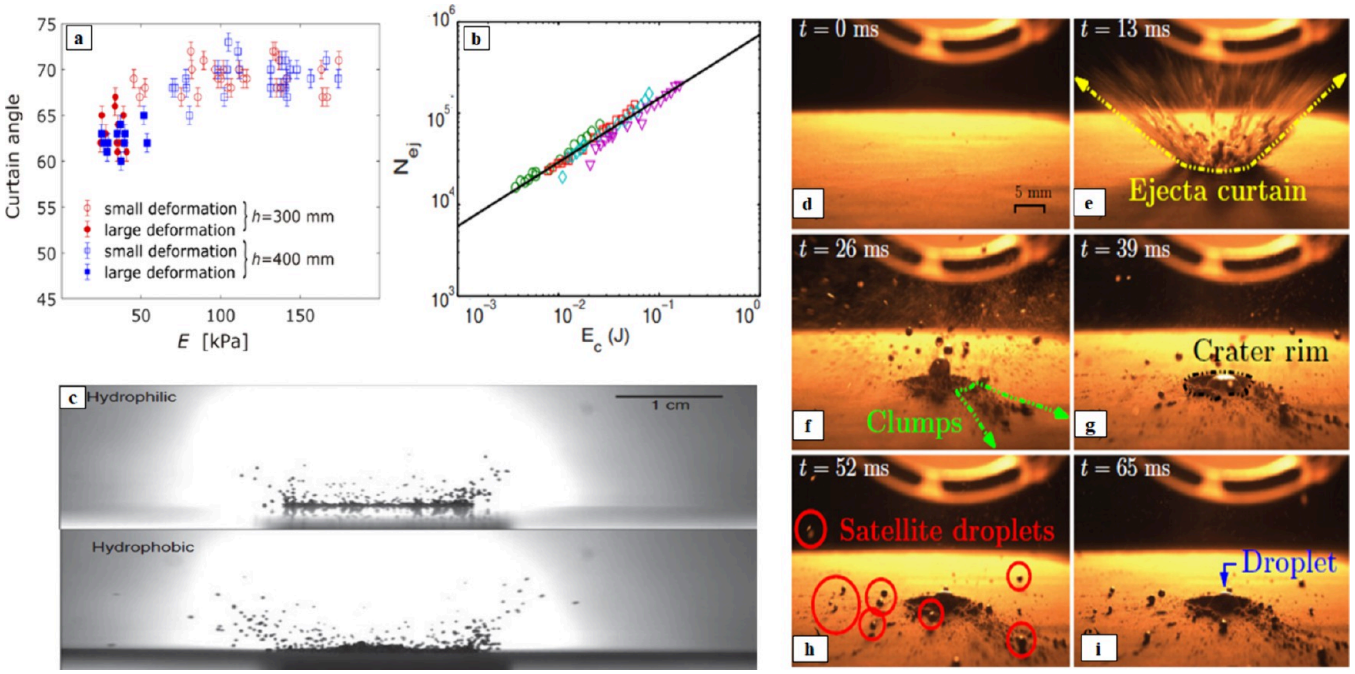

Figure 14. (a) Relationship between Young's modulus E and the ejected curtain angle. Reprinted with permission from ref 223. Copyright 2020 American Institute of Physics Publishing. (b) Number of ejected grains N_{ej} as a function of impact energy. Reprinted with permission from ref 108. Copyright 2009 American Physical Society. (c) Ejecting particles 0.30 s after a water drop impact for hydrophilic (top) and hydrophobic (bottom) particle beds. Reprinted with permission from ref 224. Copyright 2013 Wiley. (d–i) Representative sequence for an impact on an intermediate initial packing. Reprinted with permission from authors of ref 225. Copyright 2019 Springer Nature.

diameters. However, crater depth was shallower in all the cases due to the adsorption of grains on the hydrogel sphere.[217]

Next, the morphology of craters and the formation of granular residues are discussed with respect to various factors. The crater shape changes from a sink to a bump-type crater with high impact velocity and large grain sizes[188] (Figure 13g). Highly viscous liquids changed the shape of the crater due to resistance to absorption of grains and formed a smooth concave crater. The crater shape is also dependent on the characteristics of the granular bed such as particle size, wettability of grains, and the packing fraction.[212,218] Rich morphology of granular residues were seen in the report of Zhao et al.[213] and also reported in these works.[218,219] The morphology of granular residues changes from ring-shaped granular residues at low E, solid-shaped residues resembling LMs at intermediate E, and asymmetric granular residues at high energy[213] (Figure 13a–f).

Next, the effect of packing fraction and nature of powder on the granule structure was highlighted.[212,220] Fine, cohesive, and loosely packed powders led to the tunneling of the drop leading to a round-shaped granule. On the other hand, particles with high packing fraction led to the spreading of drop at lower heights forming flat discs.[220] Next, Marston et al.[162] showed an influence of both impact velocity and packing fraction on the final appearance of granule nucleus. The formation of ring-shaped granular residues occurred here in the case of loosely packed beds showing that the granule may have attained internal voidage during nucleation. At higher velocities, large numbers of satellite drops form which serve as granule nucleation sites. de Jong et al.[221] also showed the formation of a doughnut to truffle to pancake shape with both increasing velocity and packing fraction (Figure 13h).

While there was a conclusive effect of the packing fraction on granule morphology, the effects of a loose bed need to be discussed. Recently, a critical packing fraction was identified above which the granular bed would dilate under forcing. However, a dilatancy onset occurs for loose beds after droplet impact where the bed is compressed to a critical packing fraction and undergoes flow. This reasoning is used to explain the higher excavated crater volume in the case of droplet intruders as compared to solid sphere intruders.[216] Lastly, with the introduction of liquid saturation in the granular bed, droplet impact characteristics changed. Retraction, formation of ejecta, and crater formation are deeply affected by a minimal level of 1% saturation.[222]

Finally, the nature of ejecta formed as a result of crater formation is discussed. Debouef et al.[108] showed that this ejecta curtain has a constant angle with the granular surface. As anticipated, the number of ejecta grains is proportional to the energy supplied by impact (Figure 14b). Next, Wyser et al.[225] showed how ejecta was dependent on the packing fraction of granular bed as well as particle–particle interactions (Figure 14d–i). Matsuda et al.[223] reported on the nature of ejecta after the impact of a hydrogel sphere on a granular bed. The angle of the ejected curtain seemed to be independent of the free-fall heights and dependent on Young's modulus of the sphere (Figure 14a). The ejecta possessed high energy which contributes to the excavation of craters. However, it was reported earlier that all impact energy is not converted into excavating, but dissipated into interparticle collisions of granular material as well.[226] Furthermore, Ahn et al.[224] studied particle ejecta formed as a result of drop impact on hydrophobic and hydrophilic glass beads with the prerequisite of soil erosion during rainfall. Hydrophobic particles had a greater ejection angle, traveled long distances away from the site of impact, and the number of such particles was greater (Figure 14c). However, prewetted particles had fewer such

https://doi.org/10.1021/acsomega.3c07657
ACS Omega 2024, 9, 12307–12330

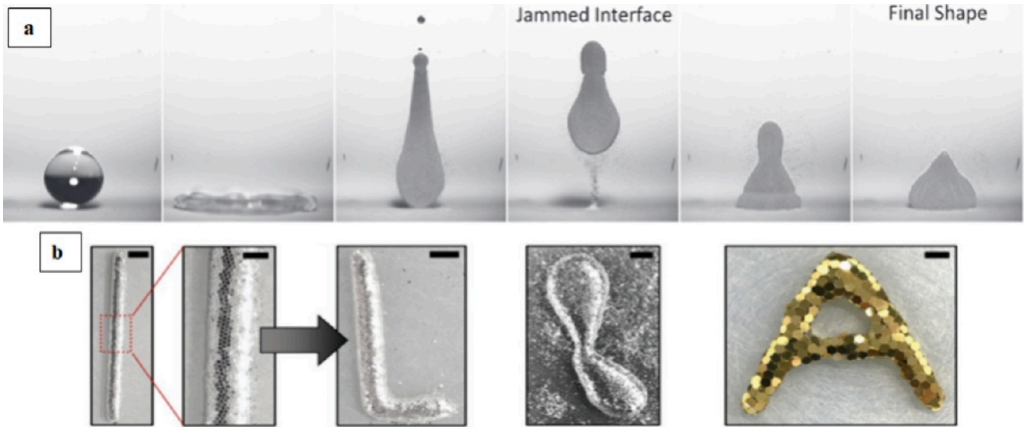

Figure 15. (a) Arrested shapes formed during the impact of 2 mm water droplets on granular beds of hydrophobic 25 μm particles. Reprinted with permission from ref 80. Copyright 2016 Elsevier. (b) Cylindrically jammed LMs formed with PET hexagonal plates showing flexibility of LM shell. Reprinted with permission from ref 230. Copyright 2019 Wiley.

incidences which had direct applications in climate-dependent soil erosion.

4.5. The Jammed State of LMs - a Peculiar Interfacial Phenomena. The first report of droplet forming frozen/deformed shapes during impact on the powder bed was reported by Marston et al.[227] At high velocities, the drop transitioned to nonspherical shapes after retraction of the drop on the powder bed. Here, the drop attained a jammed shape as the concentration of particles in the spreading lamella increased and thus underwent damped oscillations due to an increase in the weight of such LMs[213] (Figure 15a). Also during retraction, the drop undergoes jetting where this satellite drop may not coalesce with the parent drop thus reducing the drop area further and increasing the chances of adsorbing excess quantity of powder than which the drop can accommodate ($D_{max} > 1.67D_o$).[80,227] Next, the impact of LMs prepared with fine 25 μm hydrophobized glass beads led to arrested jammed shapes due to high coverage of LMs.[228] Circularity estimated before and after the impact of LM on a hydrophobic surface had decreased. Interestingly, switching of the LM axes during such a rebound is seen to be common—from a prolate to an oblate shape.[228] Further, a dilatational surface viscosity can be used to describe these jammed structures of LMs.[187] A modification of the regime map by Mozhi Devan Padmanathan et al.[33] was given. A drop impacting on a powder bed can have no encapsulation, encapsulation, spherical LMs, deformed LMs, and splashing. While drop impact on SH surfaces led to reproducible drop shapes during rebound, such shapes lacked uniformity in the case of drop impact on powder beds. This is because understanding the amount of coating that goes into LMs at high *We* numbers remains a challenge due to local jamming effects. This has been observed for a viscous PEO drop impacting a NP bed leading to sharp protrusions in the arrested drop.[229]

Jammed LMs can also be produced by rolling and manipulation of either the nature of core liquid or the chemistry of the coating particles. Singha et al.[3] formed such LMs with a combination of low surface tension and high rotation speeds similar to the use of high-impact energy in the case of drop impact on powder beds. These LMs were formed when the specific interfacial area became comparable to the close packing of particles. In other reports, cylindrical LMs were prepared by rolling with hexagonal PET plates by tuning the plate diameter and water droplet diameter and decreasing the surface tension of core liquid[230] (Figure 16b). Though it

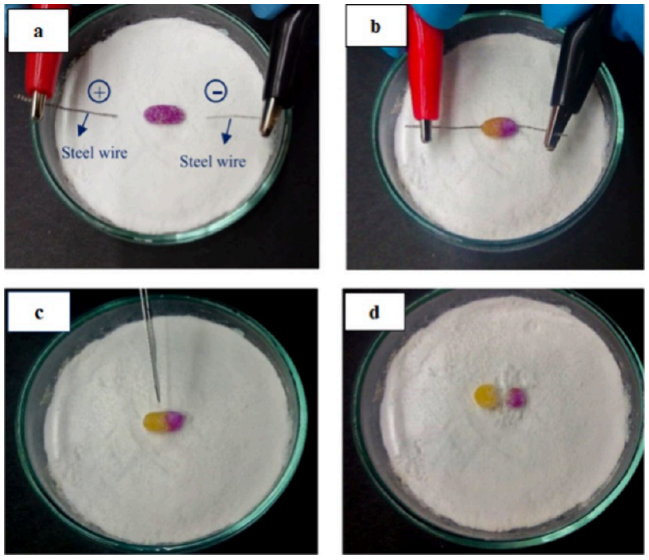

Figure 16. (a) Working of a puddle-shaped microreactor LM before insertion of electrodes. (b–d) Appearance of colored compartments which can be segmented. Reproduced with permission from ref 211. Copyright 2019. American Chemical Society.

was possible to form inelastic LMs, they were not thermodynamically stable and relaxed into spherical shapes on adsorption of water vapor. Recently, reversible jamming transitions by an increase in core volume have been used to activate LMs to coalesce and transfer liquid to another closely associated LM. Patchworks were formed on LM thus enhancing it with functionalities of multiple particles.[231] Other routes included gel-based stearic acid particles which allow irreversible deformation of a shell of LMs based on rolling time and pH of solution.[211] These LMs were demonstrated to show mini chemical reactions with a change in pH of cresol red with electric current. Here, a fascinating property of these jammed LMs was demonstrated known as "segmentation feasibility" as seen by the clear separation of varied colored LMs from a single jammed LM[211] (Figure 16a–d). Extending the idea of the shape-designability of LMs

https://doi.org/10.1021/acsomega.3c07657
ACS Omega 2024, 9, 12307−12330

prepared with liquid plasticines, liquid pancakes could also be prepared. Due to the special sol−gel layer imparted by these plasticine structures, these pancakes can be tailored to a specific shape by controlling the jamming density of the particles.[232] These approaches diversify the engineering approaches for LM fabrication.

On another note, such jammed shapes were also realized in the case of bubbles, droplets, and emulsions. Nonspherical bubbles were prepared by adsorption of a close-packed monolayer of particles, and particles could be rearranged leading to specific arrested shapes.[233] Additionally, emulsions clad with NPs allow *in situ* assembly of surfactants, which stabilize the interface against desorption like conventional surfactants.[234] These jammed particles can be stimulated by electric and magnetic fields for further shape functionality.

5. SUMMARY AND FUTURE PERSPECTIVES

LMs are versatile soft matter systems contributing to the development of a wide variety of applications. Interfacial aspects of LMs revealed a stable CB state formed by the adsorption of particles and a hierarchical roughness due to the arrangement of particles and air pockets. Similarly, bare droplet wettability was dependent on the topology of the SH surface in terms of density, shape, and size of pillars. WTs in the case of such droplets demonstrated the stability of fabricated SH surfaces. In addition to serving as a test of stability, WTs of LMs displayed the on-demand release of core liquids upon specific stimuli. Studies characterizing LM WTs with parameters such as particle size and the arrangement of particles at the interface are lacking. Next, the stability of LMs is characterized by effective surface tension which provides a macroscopic estimation of the interparticle forces. LMs performed superiorly to that of droplets during evaporation as well as compression. Here, the topology of the SH surface and the roughness and arrangement of particle clusters played a similar role. Clues regarding enhanced stability of certain particles and their arrangements might lead to deeper probing of capillary forces[74,235] Also, insights into particle rafts and packing into uniform arrangements raise queries about correlation to that of particle interactions.[143]

Understanding the dynamics of spreading phenomena builds knowledge of nucleation and granulation valuable for the pharmaceutical industry.[236] Each step in the drop impact phenomena of both flat and powder surfaces is studied and then comparatively analyzed. Comparing dimensionless scaling showed various ranges for flat and powder surfaces. However, this scaling failed for both flat and powder beds due to negligence of roughness/packing fraction. In addition to development of robust energy balance models for that of droplet impact on granular surfaces, capturing lamella dynamics such as estimation of local *We* numbers is also needed.[237] Next, the rebound phenomenon was further subdivided into retraction, jetting, and bouncing. Various additives were identified to arrest each phenomenon, and their ensuing applications were also pinpointed. While drop impact on granular surfaces was studied in the case of bouncing and jetting, there was a lack of understanding of dynamic CA changes of this coated lamella during retraction. The concept of excess energy proved crucial in predicting the occurrence of rebound on both types of surfaces. The case of surface oscillations of drop or LM at rest as well as rolling of drop/LM from its original location needs to be further checked in terms of remaining energy in the drop. A variety of splashing phenomena was observed on flat surfaces; however, the formation of fingers and shattering was the main observation in the case of granular beds. Also, there was a need to control the number of satellite drops formed on both types of surfaces. In the case of nucleation, macroscopic patterns can be introduced on beds, leading to a controllable set of satellite droplets. Splashing parameter K was higher in the case of granular beds as compared to that of flat surfaces due to damping. Additionally, completely coated LMs were obtained when the maximum spread ratio was greater than 2 with the occurrence of a positive excess energy. Variations in crater morphology in terms of particle sizes, impact velocities, and packing fraction showed the formation of rings and asymmetric residues. The consequences of ejecta formation were identified in the soil environment consisting of a mixture of particle wettabilities. Finally, a critical impact velocity showed the formation of jammed LMs. The flexibility of liquid plasticines and the formation of compartments have potential implications for conducting multiple microreactions inside a single LM. Recently, Janus LMs have been fabricated using droplet impact, which accentuated the need for a deep understanding of the flows leading to the formation of a fixed particle crest.[238] Lastly, considering the potential of innovative application aspects of these LMs, unexplored *We* and *Re* ranges could yield interesting patterns and tailored coatings.

AUTHOR INFORMATION

Corresponding Author

Sameer Dalvi − *Chemical Engineering, Indian Institute of Technology Gandhinagar, Palaj, Gandhinagar 382055 Gujarat, India;* orcid.org/0000-0001-5262-8711; Phone: 091-79-2395240; Email: sameervd@iitgn.ac.in

Author

Apoorva Sneha Ravi − *Chemical Engineering, Indian Institute of Technology Gandhinagar, Palaj, Gandhinagar 382055 Gujarat, India*

Complete contact information is available at: https://pubs.acs.org/10.1021/acsomega.3c07657

Notes

The authors declare no competing financial interest.

ACKNOWLEDGMENTS

The authors gratefully acknowledge financial support from the Ministry of Human Resource and Development of the Government of India and the Indian Institute of Technology Gandhinagar (IITGN).

ABBREVIATIONS:

LM	liquid marble
CB	Cassie−Baxter
WT	wetting transition
PTFE	polytetrafluoroethylene
PVDF	polyvinylidenefluoride
PE	polyethylene
SH	superhydrophobic
NP	nanoparticle
CA	contact angle
CCA	constant contact angle
CCR	constant contact radius
RH	relative humidity

https://doi.org/10.1021/acsomega.3c07657
ACS Omega 2024, 9, 12307−12330

PDDA	polydiallyldimethyl ammonium chloride
DNA	deoxyribonucleic acid
PCR	polymerase chain reaction
PET	polyethylene terephthalate
SLIPS	slippery liquid infused porous surfaces
UV	ultraviolet
CMC	critical micelle concentration
SDS	sodium dodecyl sulfate
ESEM	environmental scanning electron microscopy
PMSQ	polymethyl silsesquioxane
CNT	carbon nanotube
HMDS	hexamethyl disilazane
DMDCS	dimethyl dichlorosilane
S−H	Schimdt−Holsapple

REFERENCES

(1) Aussillous, P.; Quéré, D. Liquid Marbles. *Nature* **2001**, *411* (6840), 924−927.

(2) Bormashenko, E.; Pogreb, R.; Musin, A.; Balter, R.; Whyman, G.; Aurbach, D. Interfacial and Conductive Properties of Liquid Marbles Coated with Carbon Black. *Powder Technol.* **2010**, *203* (3), 529−533.

(3) Singha, P.; Nguyen, N.-K.; Sreejith, K. R.; An, H.; Nguyen, N.-T.; Ooi, C. H. Surface Tension: Effect of Core Liquid Surface Tension on the Liquid Marble Shell (Adv. Mater. Interfaces 5/2021). *Adv. Mater. Interfaces* **2021**, *8* (5), No. 2170025.

(4) Nguyen, T. H.; Hapgood, K.; Shen, W. Observation of the Liquid Marble Morphology Using Confocal Microscopy. *Chem. Eng. J.* **2010**, *162* (1), 396−405.

(5) Fujii, S.; Suzaki, M.; Armes, S. P.; Dupin, D.; Hamasaki, S.; Aono, K.; Nakamura, Y. Liquid Marbles Prepared from PH-Responsive Sterically Stabilized Latex Particles. *Langmuir* **2011**, *27* (13), 8067−8074.

(6) Asaumi, Y.; Rey, M.; Vogel, N.; Nakamura, Y.; Fujii, S. Particle Monolayer-Stabilized Light-Sensitive Liquid Marbles from Polypyrrole-Coated Microparticles. *Langmuir* **2020**, *36* (10), 2695.

(7) Tosun, A.; Erbil, H. Y. Evaporation Rate of PTFE Liquid Marbles. *Appl. Surf. Sci.* **2009**, *256* (5), 1278−1283.

(8) Bormashenko, E.; Bormashenko, Y.; Musin, A.; Barkay, Z. On the Mechanism of Floating and Sliding of Liquid Marbles. *ChemPhysChem* **2009**, *10* (4), 654−656.

(9) Ravi, A. S.; Dalvi, S. V. Unraveling Stability of a Floating Liquid Marble, Its Opening and Resulting Collapse Patterns. *Colloids Surfaces A Physicochem. Eng. Asp.* **2022**, *648*, No. 129347.

(10) Rendos, A.; Alsharif, N.; Kim, B. L.; Brown, K. A. Elasticity and Failure of Liquid Marbles: Influence of Particle Coating and Marble Volume. *Soft Matter* **2017**, *13* (47), 8903−8909.

(11) Dandan, M.; Erbil, H. Y. Evaporation Rate of Graphite Liquid Marbles: Comparison with Water Droplets. *Langmuir* **2009**, *25* (14), 8362−8367.

(12) Bormashenko, E.; Bormashenko, Y. Non-Stick Droplet Surgery with a Superhydrophobic Scalpel. *Langmuir* **2011**, *27* (7), 3266−3270.

(13) Luo, X.; Yin, H.; Li, X.; Su, X.; Feng, Y. CO_2-Triggered Microreactions in Liquid Marbles. *Chem. Commun.* **2018**, *54* (66), 9119−9122.

(14) Pike, N.; Richard, D.; Foster, W.; Mahadevan, L. How Aphids Lose Their Marbles. *Proc. R. Soc. B Biol. Sci.* **2002**, *269* (1497), 1211−1215.

(15) Cassie, A. B. D. Contact Angles. *Discussions of the Faraday Society*. **1948**, 3, 11.

(16) Kasahara, M.; Akimoto, S. I.; Hariyama, T.; Takaku, Y.; Yusa, S. I.; Okada, S.; Nakajima, K.; Hirai, T.; Mayama, H.; Okada, S.; et al. Liquid Marbles in Nature: Craft of Aphids for Survival. *Langmuir* **2019**, *35*, 6169.

(17) Barthlott, W.; Neinhuis, C. Purity of the Sacred Lotus, or Escape from Contamination in Biological Surfaces. *Planta* **1997**, *202* (1), 1−8.

(18) Singha, P.; Swaminathan, S.; Yadav, A. S.; Varanakkottu, S. N. Surfactant-Mediated Collapse of Liquid Marbles and Directed Assembly of Particles at the Liquid Surface. *Langmuir* **2019**, *35* (13), 4566−4576.

(19) Dupin, D.; Armes, S. P.; Fujii, S. Stimulus-Responsive Liquid Marbles. *J. Am. Chem. Soc.* **2009**, *131* (15), 5386−5387.

(20) Frenkel, M.; Dombrovsky, L.; Multanen, V.; Danchuk, V.; Legchenkova, I.; Shoval, S.; Bormashenko, Y.; Binks, B. P.; Bormashenko, E. Self-Propulsion of Water-Supported Liquid Marbles Filled with Sulfuric Acid. *J. Phys. Chem. B* **2018**, *122*, 7936−7942, DOI: 10.1021/acs.jpcb.8b06136.

(21) Ooi, C. H.; Van Nguyen, A.; Evans, G. M.; Gendelman, O.; Bormashenko, E.; Nguyen, N. T. A Floating Self-Propelling Liquid Marble Containing Aqueous Ethanol Solutions. *RSC Adv.* **2015**, *5* (122), 101006−101012.

(22) Paven, M.; Mayama, H.; Sekido, T.; Butt, H. J. J.; Nakamura, Y.; Fujii, S. Light-Driven Delivery and Release of Materials Using Liquid Marbles. *Adv. Funct. Mater.* **2016**, *26* (19), 3199−3206.

(23) Vadivelu, R. K.; Ooi, C. H.; Yao, R. Q.; Tello Velasquez, J.; Pastrana, E.; Diaz-Nido, J.; Lim, F.; Ekberg, J. A. K.; Nguyen, N. T.; St John, J. A. Generation of Three-Dimensional Multiple Spheroid Model of Olfactory Ensheathing Cells Using Floating Liquid Marbles. *Sci. Rep.* **2015**, *5* (1), 1−12.

(24) Vadivelu, R. K.; Kamble, H.; Munaz, A.; Nguyen, N. T. Liquid Marbles as Bioreactors for the Study of Three-Dimensional Cell Interactions. *Biomed. Microdevices* **2017**, *19* (2), 1−9.

(25) Arbatan, T.; Li, L.; Tian, J.; Shen, W. Liquid Marbles as Micro-Bioreactors for Rapid Blood Typingy. *Adv. Healthc. Mater.* **2012**, *1* (1), 80−83.

(26) Miao, Y. E.; Lee, H. K.; Chew, W. S.; Phang, I. Y.; Liu, T.; Ling, X. Y. Catalytic Liquid Marbles: Ag Nanowire-Based Miniature Reactors for Highly Efficient Degradation of Methylene Blue. *Chem. Commun.* **2014**, *50* (44), 5923−5926.

(27) Tian, J.; Arbatan, T.; Li, X.; Shen, W. Porous Liquid Marble Shell Offers Possibilities for Gas Detection and Gas Reactions. *Chem. Eng. J.* **2010**, *165* (1), 347−353.

(28) Lekshmi, B. S.; Varanakkottu, S. N. Droplet-Impact Driven Formation of Ultralow Volume Liquid Marbles with Enhanced Mechanical Stability and Sensing Ability. *Langmuir* **2022**, *38* (38), 11743−11752.

(29) Bormashenko, E.; Stein, T.; Whyman, G.; Bormashenko, Y.; Pogreb, R. Wetting Properties of the Multiscaled Nanostructured Polymer and Metallic Superhydrophobic Surfaces. *Langmuir* **2006**, *22* (24), 9982−9985.

(30) Eshtiaghi, N.; Hapgood, K. P. A Quantitative Framework for the Formation of Liquid Marbles and Hollow Granules from Hydrophobic Powders. *Powder Technol.* **2012**, *223*, 65−76.

(31) Saleh, K.; Forny, L.; Guigon, P.; Pezron, I. Dry Water: From Physico-Chemical Aspects to Process-Related Parameters. *Chem. Eng. Res. Des.* **2011**, *89* (5), 537−544.

(32) Yue, S.; Shen, W.; Hapgood, K. Characterisation of Liquid Marbles in Commercial Cosmetic Products. *Adv. Powder Technol.* **2016**, *27* (1), 33−41.

(33) Mozhi Devan Padmanathan, A.; Sneha Ravi, A.; Choudhary, H.; Varanakkottu, S. N.; Dalvi, S. V. Predictive Framework for the Spreading of Liquid Drops and the Formation of Liquid Marbles on Hydrophobic Particle Bed. *Langmuir* **2019**, *35* (20), 6657−6668.

(34) Eshtiaghi, N.; Liu, J. S.; Shen, W.; Hapgood, K. P. Liquid Marble Formation: Spreading Coefficients or Kinetic Energy? *Powder Technol.* **2009**, *196* (2), 126−132.

(35) Bormashenko, E. Liquid Marbles: Properties and Applications. *Curr. Opin. Colloid Interface Sci.* **2011**, *16* (4), 266−271.

(36) McHale, G.; Newton, M. I. Liquid Marbles: Principles and Applications. *Soft Matter* **2011**, *7* (12), 5473−5481.

(37) Bormashenko, E. Liquid Marbles, Elastic Nonstick Droplets: From Minireactors to Self-Propulsion. *Langmuir* **2017**, *33* (3), 663−669.

https://doi.org/10.1021/acsomega.3c07657
ACS Omega 2024, 9, 12307−12330

(38) Sun, Y.; Zheng, Y.; Liu, C.; Zhang, Y.; Wen, S.; Song, L.; Zhao, M. Liquid Marbles, Floating Droplets: Preparations, Properties, Operations and Applications. *RSC Adv.* **2022**, *12* (24), 15296−15315.
(39) McHale, G.; Newton, M. I. Liquid Marbles: Topical Context within Soft Matter and Recent Progress. *Soft Matter* **2015**, *11* (13), 2530−2546.
(40) Avrămescu, R. E.; Ghica, M. V.; Dinu-Pîrvu, C.; Udeanu, D. I.; Popa, L. Liquid Marbles: From Industrial to Medical Applications. *Molecules.* **2018**, *23*, 1120.
(41) Saczek, J.; Yao, X.; Zivkovic, V.; Mamlouk, M.; Wang, D.; Pramana, S. S.; Wang, S. Long-Lived Liquid Marbles for Green Applications. *Adv. Funct. Mater.* **2021**, *31* (35), No. 2011198.
(42) Singha, P.; Ooi, C. H.; Nguyen, N. K.; Sreejith, K. R.; Jin, J.; Nguyen, N. T. Capillarity: Revisiting the Fundamentals of Liquid Marbles. *Microfluidics and Nanofluidics.* **2020**, DOI: 10.1007/s10404-020-02385-9.
(43) Pickering, S. U. CXCVI. - Emulsions. *J. Chem. Soc, Trans.* **1907**, *91*, 2001−2021, DOI: 10.1039/CT9079102001.
(44) Ramsden, W. Separation of Solids in the Surface-Layers of Solutions and 'Suspensions' (Observations on Surface-Membranes, Bubbles, Emulsions, and Mechanical Coagulation).—Preliminary Account. *Proc. R. Soc. London* **1904**, *72* (477−486), 156−164, DOI: 10.1098/rspl.1903.0034.
(45) Garbin, V. Colloidal Particles: Surfactants with a Difference. *Phys. Today* **2013**, *66*, 68.
(46) Binks, B. P. Particles as Surfactants - Similarities and Differences. *Curr. Opin. Colloid Interface Sci.* **2002**, *7* (1−2), 21−41.
(47) Binks, B. P.; Murakami, R. Phase Inversion of Particle-Stabilized Materials from Foams to Dry Water. *Nat. Mater.* **2006**, *5* (11), 865−869.
(48) Finkle, P.; Draper, H. D.; Hildebrand, J. H. The Theory of Emulsification. *J. Am. Chem. Soc.* **1923**, *45* (12), 2780−2788.
(49) Fletcher, P. D. I.; Holt, B. L. Controlled Silanization of Silica Nanoparticles to Stabilize Foams, Climbing Films, and Liquid Marbles. *Langmuir* **2011**, *27* (21), 12869−12876.
(50) Whitby, C. P.; Bian, X.; Sedev, R. Spontaneous Liquid Marble Formation on Packed Porous Beds. *Soft Matter* **2012**, *8* (44), 11336−11342.
(51) Forny, L.; Pezron, I.; Saleh, K.; Guigon, P.; Komunjer, L. Storing Water in Powder Form by Self-Assembling Hydrophobic Silica Nanoparticles. *Powder Technol.* **2007**, *171* (1), 15−24.
(52) Kralchevsky, P. A.; Nagayama, K. Capillary Forces between Colloidal Particles. *Langmuir* **1994**, *10*, 23.
(53) Bormashenko, E.; Pogreb, R.; Whyman, G.; Musin, A. Surface Tension of Liquid Marbles. *Colloids Surfaces A Physicochem. Eng. Asp.* **2009**, *351* (1−3), 78−82.
(54) Bormashenko, E.; Pogreb, R.; Whyman, G.; Musin, A.; Bormashenko, Y.; Barkay, Z. Shape, Vibrations, and Effective Surface Tension of Water Marbles. *Langmuir* **2009**, *25* (4), 1893−1896.
(55) Bormashenko, E.; Musin, A.; Whyman, G.; Barkay, Z.; Starostin, A.; Valtsifer, V.; Strelnikov, V. Revisiting the Surface Tension of Liquid Marbles: Measurement of the Effective Surface Tension of Liquid Marbles with the Pendant Marble Method. *Colloids Surfaces A Physicochem. Eng. Asp.* **2013**, *425*, 15−23.
(56) Arbatan, T.; Shen, W. Measurement of the Surface Tension of Liquid Marbles. *Langmuir* **2011**, *27* (21), 12923−12929.
(57) Singha, P.; Nguyen, N. K.; Zhang, J.; Nguyen, N. T.; Ooi, C. H. Oscillating Sessile Liquid Marble - A Tool to Assess Effective Surface Tension. *Colloids Surfaces A Physicochem. Eng. Asp.* **2021**, *627*, No. 127176.
(58) Planchette, C.; Lorenceau, E.; Biance, A.-L. L. Surface Wave on a Particle Raft. *Soft Matter* **2012**, *8* (8), 2444.
(59) Monteux, C.; Kirkwood, J.; Xu, H.; Jung, E.; Fuller, G. G. Determining the Mechanical Response of Particle-Laden Fluid Interfaces Using Surface Pressure Isotherms and Bulk Pressure Measurements of Droplets. *Phys. Chem. Chem. Phys.* **2007**, *9* (48), 6344−6350.
(60) Li, X.; Wang, R.; Huang, S.; Wang, Y.; Shi, H. A Capillary Rise Method for Studying the Effective Surface Tension of Monolayer Nanoparticle-Covered Liquid Marbles. *Soft Matter* **2018**, *14*, 9877.
(61) Singha, P.; Nguyen, N. K.; Nguyen, V. T.; Sreejith, K. R.; Tran, D. T.; Nguyen, A. V.; Nguyen, N. T.; Ooi, C. H. Investigation of Liquid Marble Shell Using X-Ray: Shell Thickness and Effective Surface Tension. *ChemNanoMat* **2022**, *8* (1). DOI: 10.1002/cnma.202100423.
(62) Wang, R.; Li, X. On the Effective Surface Tension of Powder-Derived Liquid Marbles. *Powder Technol.* **2020**, *367*, 608.
(63) Ooi, C. H.; Vadivelu, R.; Jin, J.; Sreejith, K. R.; Singha, P.; Nguyen, N. K. N. T.; Nguyen, N. K. N. T. Liquid Marble-Based Digital Microfluidics − Fundamentals and Applications. *Lab Chip* **2021**, *21* (7), 1199−1216.
(64) Vella, D.; Mahadevan, L. The "Cheerios Effect. *Am. J. Phys.* **2005**, *73*, 817.
(65) Larmour, I. A.; Saunders, G. C.; Bell, S. E. J. Sheets of Large Superhydrophobic Metal Particles Self Assembled on Water by the Cheerios Effect. *Angew. Chemie - Int. Ed.* **2008**, *47*, 5043.
(66) Cengiz, U.; Erbil, H. Y. The Lifetime of Floating Liquid Marbles: The Influence of Particle Size and Effective Surface Tension. *Soft Matter* **2013**, *9* (37), 8980−8991.
(67) Zang, D.; Chen, Z.; Zhang, Y.; Lin, K.; Geng, X.; Binks, B. P. Effect of Particle Hydrophobicity on the Properties of Liquid Water Marbles. *Soft Matter* **2013**, *9* (20), 5067−5073.
(68) Celestini, F.; Kofman, R. Vibration of Submillimeter-Size Supported Droplets. *Phys. Rev. E - Stat. Nonlinear, Soft Matter Phys.* **2006**, *73* (4), No. 041602.
(69) Monteux, C.; Kirkwood, J.; Xu, H.; Jung, E.; Fuller, G. G. Determining the Mechanical Response of Particle-Laden Fluid Interfaces Using Surface Pressure Isotherms and Bulk Pressure Measurements of Droplets. *Phys. Chem. Chem. Phys.* **2007**, *9* (48), 6344−6350.
(70) Monteux, C.; Jung, E.; Fuller, G. G. Mechanical Properties and Structure of Particle Coated Interfaces: Influence of Particle Size and Bidisperse 2D Suspensions. *Langmuir* **2007**, *23* (7), 3975−3980.
(71) Bormashenko, E.; Balter, R.; Aurbach, D. Micropump Based on Liquid Marbles. *Appl. Phys. Lett.* **2010**, *97* (9), No. 091908.
(72) Stamou, D.; Duschl, C.; Johannsmann, D. Long-Range Attraction between Colloidal Spheres at the Air-Water Interface: The Consequence of an Irregular Meniscus. *Phys. Rev. E - Stat. Physics, Plasmas, Fluids, Relat. Interdiscip. Top.* **2000**, *62* (4), 5263−5272.
(73) Hapgood, K. P.; Khanmohammadi, B. Granulation of Hydrophobic Powders. *Powder Technol.* **2009**, *189* (2), 253−262.
(74) Bhosale, P. S.; Panchagnula, M. V.; Stretz, H. A. Mechanically Robust Nanoparticle Stabilized Transparent Liquid Marbles. *Appl. Phys. Lett.* **2008**, *93* (3), 1−3.
(75) Eshtiaghi, N.; Liu, J. J. S.; Hapgood, K. P. Formation of Hollow Granules from Liquid Marbles: Small Scale Experiments. *Powder Technol.* **2010**, *197* (3), 184−195.
(76) Gao, L.; McCarthy, T. J. Ionic Liquid Marbles. *Langmuir* **2007**, *23* (21), 10445−10447.
(77) Hapgood, K. P.; Farber, L.; Michaels, J. N. Agglomeration of Hydrophobic Powders via Solid Spreading Nucleation. *Powder Technol.* **2009**, *188* (3), 248−254.
(78) McEleney, P.; Walker, G. M.; Larmour, I. A.; Bell, S. E. J. Liquid Marble Formation Using Hydrophobic Powders. *Chem. Eng. J.* **2009**, *147* (2−3), 373−382.
(79) Ireland, P. M.; Noda, M.; Jarrett, E. D.; Fujii, S.; Nakamura, Y.; Wanless, E. J.; Webber, G. B. Electrostatic Formation of Liquid Marbles - Influence of Drop and Particle Size. *Powder Technol.* **2016**, *303*, 55−58.
(80) Supakar, T.; Moradiafrapoli, M.; Christopher, G. F.; Marston, J. O. Spreading, Encapsulation and Transition to Arrested Shapes during Drop Impact onto Hydrophobic Powders. *J. Colloid Interface Sci.* **2016**, *468*, 10−20.
(81) Wenzel, R. N. Resistance of Solid Surfaces to Wetting by Water. *Ind. Eng. Chem.* **1936**, *28*, 988.

(82) Schwartz, A. M.; Perry, J. W. *Surface Active Agents*; Interscience Publishers, 1949.
(83) Cassie, A. B. D.; Baxter, S. Wettability of Porous Surfaces. *Trans. Faraday Soc.* **1944**, *40*, 546.
(84) Lafuma, A.; Quéré, D. Superhydrophobic States. *Nat. Mater.* **2003**, *2*, 457.
(85) Bico, J.; Marzolin, C.; Quéré, D. Pearl Drops. *Europhys. Lett.* **1999**, *47* (6), 743−744.
(86) Shirtcliffe, N. J.; McHale, G.; Atherton, S.; Newton, M. I. An Introduction to Superhydrophobicity. *Adv. Colloid Interface Sci.* **2010**, *161* (1−2), 124−138.
(87) Patankar, N. A. Transition between Superhydrophobic States on Rough Surfaces. *Langmuir* **2004**, *20*, 7097.
(88) Lee, C.; Nam, Y.; Lastakowski, H.; Hur, J. I.; Shin, S.; Biance, A. L.; Pirat, C.; Kim, C. J.; Ybert, C. Two Types of Cassie-to-Wenzel Wetting Transitions on Superhydrophobic Surfaces during Drop Impact. *Soft Matter* **2015**, *11* (23), 4592−4599.
(89) Callies, M.; Quéré, D. On Water Repellency. *Soft Matter* **2005**, *1* (1), 55−61.
(90) Bussonnière, A.; Bigdeli, M. B.; Chueh, D. Y.; Liu, Q.; Chen, P.; Tsai, P. A. Universal Wetting Transition of an Evaporating Water Droplet on Hydrophobic Micro- and Nano-Structures. *Soft Matter* **2017**, *13* (5), 978−984.
(91) Smyth, K.; Paxon, A.; Kwon, H. M.; Deng, T.; Varanasi, K. K. Dynamic Wetting on Superhydrophobic Surfaces: Droplet Impact and Wetting Hysteresis *12th IEEE Intersociety Conference on Thermal and Thermomechanical Phenomena in Electronic Systems*, 2010. DOI: 10.1109/ITHERM.2010.5501329
(92) Kim, S. H. Fabrication of Superhydrophobic Surfaces. *J. Adhesion Sci. Technol.* **2012**, *22* (3-4), 235−250, DOI: 10.1163/156856108X305156.
(93) Öner, D.; McCarthy, T. J. Ultrahydrophobic Surfaces. Effects of Topography Length Scales on Wettability. *Langmuir* **2000**, *16* (20), 7777−7782.
(94) Shirtcliffe, N. J.; McHale, G.; Newton, M. I.; Chabrol, G.; Perry, C. C. Dual-Scale Roughness Produces Unusually Water-Repellent Surfaces. *Adv. Mater.* **2004**, *16* (21), 1929−1932.
(95) Dorrer, C.; Ruhe, J. Some Thoughts on Superhydrophobic Wetting. *Soft Matter* **2009**, *5* (1), 51−61.
(96) Whyman, G.; Bormashenko, E. How to Make the Cassie Wetting State Stable? *Langmuir* **2011**, *27* (13), 8171−8176.
(97) Papadopoulos, P.; Mammen, L.; Deng, X.; Vollmer, D.; Butt, H. J. How Superhydrophobicity Breaks Down. *Proc. Natl. Acad. Sci. U. S. A.* **2013**, *110* (9), 3254−3258.
(98) Bormashenko, E. Wetting Transitions on Biomimetic Surfaces. *Philos. Trans. R. Soc. A Math. Phys. Eng. Sci.* **2010**, *368* (1929), 4695−4711.
(99) Mahadevan, L. Soft Matter: Non-Stick Water. *Nature* **2001**, *411* (6840), 895−896.
(100) Cheng, Y. T.; Rodak, D. E. Is the Lotus Leaf Superhydrophobic? *Appl. Phys. Lett.* **2005**, *86* (14), 1−3.
(101) Vu, H. H.; Nguyen, N. T.; Kashaninejad, N. Re-Entrant Microstructures for Robust Liquid Repellent Surfaces. *Adv. Mater. Technol.* **2023**, *8* (5), No. 2201836.
(102) Chen, X.; Weibel, J. A.; Garimella, S. V. Water and Ethanol Droplet Wetting Transition during Evaporation on Omniphobic Surfaces. *Sci. Reports 2015 51* **2015**, *5* (1), 1−11.
(103) Dai, H.; Gao, C.; Sun, J.; Li, C.; Li, N.; Wu, L.; Dong, Z.; Jiang, L. Controllable High-Speed Electrostatic Manipulation of Water Droplets on a Superhydrophobic Surface. *Adv. Mater.* **2019**, *31* (43), No. 1905449.
(104) Wen, R.; Lan, Z.; Peng, B.; Xu, W.; Yang, R.; Ma, X. Wetting Transition of Condensed Droplets on Nanostructured Superhydrophobic Surfaces: Coordination of Surface Properties and Condensing Conditions. *ACS Appl. Mater. Interfaces* **2017**, *9* (15), 13770−13777.
(105) McHale, G.; Newton, M. I.; Shirtcliffe, N. J.; Geraldi, N. R. Capillary Origami: Superhydrophobic Ribbon Surfaces and Liquid Marbles. *Beilstein J. Nanotechnol.* **2011**, *2* (1), 145−151.
(106) Bormashenko, E. *Progress in Understanding Wetting Transitions on Rough Surfaces*; Elsevier, 2015; Vol. *222*, pp 92−103.
(107) Bormashenko, E.; Balter, R.; Aurbach, D. Formation of Liquid Marbles and Wetting Transitions. *J. Colloid Interface Sci.* **2012**, *384* (1), 157−161.
(108) Deboeuf, S.; Gondret, P.; Rabaud, M. Dynamics of Grain Ejection by Sphere Impact on a Granular Bed. *Phys. Rev. E* **2009**, *79* (4), No. 041306.
(109) Tan, T. T. Y.; Ahsan, A.; Reithofer, M. R.; Tay, S. W.; Tan, S. Y.; Hor, T. S. A.; Chin, J. M.; Chew, B. K. J.; Wang, X. Photoresponsive Liquid Marbles and Dry Water. *Langmuir* **2014**, *30* (12), 3448−3454.
(110) Newton, M. I.; Herbertson, D. L.; Elliott, S. J.; Shirtcliffe, N. J.; McHale, G. Electrowetting of Liquid Marbles. *J. Phys. D. Appl. Phys.* **2007**, *40* (1), 20−24.
(111) Tenjimbayashi, M.; Samitsu, S.; Naito, M. Simultaneous Detection and Repair of Wetting Defects in Superhydrophobic Coatings via Cassie−Wenzel Transitions of Liquid Marbles. *Adv. Funct. Mater.* **2019**, DOI: 10.1002/adfm.201900688.
(112) Bhushan, B.; Nosonovsky, M. The Rose Petal Effect and the Modes of Superhydrophobicity. *Philos. Trans. R. Soc. A Math. Phys. Eng. Sci.* **2010**, *368* (1929), 4713−4728.
(113) Erbil, H. Y. Evaporation of Pure Liquid Sessile and Spherical Suspended Drops: A Review. *Adv. Colloid Interface Sci.* **2012**, *170* (1−2), 67−86.
(114) Yu, Y. S.; Huang, X.; Sun, L.; Zhou, J. Z.; Zhou, A. Evaporation of Ethanol/Water Mixture Droplets on Micro-Patterned PDMS Surfaces. *Int. J. Heat Mass Transfer* **2019**, *144*, No. 118708.
(115) Xu, W.; Leeladhar, R.; Kang, Y. T.; Choi, C. H. Evaporation Kinetics of Sessile Water Droplets on Micropillared Superhydrophobic Surfaces. *Langmuir* **2013**, *29* (20), 6032−6041.
(116) Bormashenko, E.; Bormashenko, Y.; Stein, T.; Whyman, G.; Bormashenko, E. Why Do Pigeon Feathers Repel Water? Hydrophobicity of Pennae, Cassie−Baxter Wetting Hypothesis and Cassie−Wenzel Capillarity-Induced Wetting Transition. *J. Colloid Interface Sci.* **2007**, *311* (1), 212−216.
(117) Tsai, P.; Lammertink, R. G. H.; Wessling, M.; Lohse, D. Evaporation-Triggered Wetting Transition for Water Droplets upon Hydrophobic Microstructures. *Phys. Rev. Lett.* **2010**, *104* (11), No. 116102.
(118) Reyssat, M.; Yeomans, J. M.; Quéré, D. Impalement of Fakir Drops. *EPL* **2008**, *81* (2), 26006.
(119) Deegan, R. D.; Bakajin, O.; Dupont, T. F.; Huber, G.; Nagel, S. R.; Witten, T. A. Capillary Flow as the Cause of Ring Stains from Dried Liquid Drops. *Nature* **1997**, *389*, 827−829, DOI: 10.1038/39827.
(120) McBride, S. A. A.; Dash, S.; Varanasi, K. K. Evaporative Crystallization in Drops on Superhydrophobic and Liquid-Impregnated Surfaces. *Langmuir* **2018**, *34* (41), 12350−12358.
(121) Ooi, C. H.; Bormashenko, E.; Nguyen, A. V.; Evans, G. M.; Dao, D. V.; Nguyen, N. T. Evaporation of Ethanol-Water Binary Mixture Sessile Liquid Marbles. *Langmuir* **2016**, *32* (24), 6097−6104.
(122) Laborie, B.; Lachaussée, F.; Lorenceau, E.; Rouyer, F. How Coatings with Hydrophobic Particles May Change the Drying of Water Droplets: Incompressible Surface versus Porous Media Effects. *Soft Matter* **2013**, *9* (19), 4822−4830.
(123) Aberle, C.; Lewis, M.; Yu, G.; Lei, N.; Xu, J. Liquid Marbles as Thermally Robust Droplets: Coating-Assisted Leidenfrost-like Effect. *Soft Matter* **2011**, *7* (24), 11314−11318.
(124) Tuvshindorj, U.; Yildirim, A.; Ozturk, F. E.; Bayindir, M. Robust Cassie State of Wetting in Transparent Superhydrophobic Coatings. *ACS Appl. Mater. Interfaces* **2014**, *6*, 9680.
(125) Bhosale, P. S.; Panchagnula, M. V. On Synthesizing Solid Polyelectrolyte Microspheres from Evaporating Liquid Marbles. *Langmuir* **2010**, *26* (13), 10745−10749.
(126) Matsukuma, D.; Watanabe, H.; Minn, M.; Fujimoto, A.; Shinohara, T.; Jinnai, H.; Takahara, A. Preparation of Poly(Lactic-Acid)-Particle Stabilized Liquid Marble and the Improvement of Its

Stability by Uniform Shell Formation through Solvent Vapor Exposure. *RSC Adv.* **2013**, *3* (21), 7862−7866.
(127) Salehabad, S. M.; Azizian, S. Elemental Sulfur-Stabilized Liquid Marbles: Properties and Applications. *ACS Appl. Mater. Interfaces* **2020**, *12* (38), 43201−43211.
(128) Gallo, A.; Tavares, F.; Das, R.; Mishra, H. How Particle−Particle and Liquid−Particle Interactions Govern the Fate of Evaporating Liquid Marbles. *Soft Matter* **2021**, *17* (33), 7628−7644.
(129) Sheng, Y.; Sun, G.; Wu, J.; Ma, G.; Ngai, T. Silica-Based Liquid Marbles as Microreactors for the Silver Mirror Reaction. *Angew. Chem.* **2015**, *127* (24), 7118−7123.
(130) Feng, Y.; Yao, G.; Xu, J.; Wang, L.; Liu, G. Effect of Surface Roughness on the Solar Evaporation of Liquid Marbles. *J. Colloid Interface Sci.* **2023**, *629*, 644−653.
(131) Roy, P. K.; Shoval, S.; Sharabi, M.; Bormashenko, E. Soft Lithography with Liquid Marbles. *Colloids Surfaces A Physicochem. Eng. Asp.* **2020**, *607*, No. 125488.
(132) Sreejith, K. R.; Ooi, C. H.; Dao, D. V.; Nguyen, N. T. Evaporation Dynamics of Liquid Marbles at Elevated Temperatures. *RSC Adv.* **2018**, *8* (28), 15436−15443.
(133) Sreejith, K. R.; Gorgannezhad, L.; Jin, J.; Ooi, C. H.; Stratton, H.; Dao, D. V.; Nguyen, N. T. Liquid Marbles as Biochemical Reactors for the Polymerase Chain Reaction. *Lab Chip* **2019**, *19* (19), 3220−3227.
(134) Vadivelu, R.; Kashaninejad, N.; Nikmaneshi, M. R.; Khadim, R. R.; Salehi, S. S.; Ramulu, N. C.; Sakai, Y.; Nishikawa, M.; Firoozabadi, B.; Nguyen, N. T. Sessile Liquid Marbles with Embedded Hydrogels as Bioreactors for Three-Dimensional Cell Culture. *Adv. Biol.* **2021**, *5* (2), No. 2000108.
(135) Yao, X.; Chen, Q.; Xu, L.; Li, Q.; Song, Y.; Gao, X.; Quéré, D.; Jiang, L. Bioinspired Ribbed Nanoneedles with Robust Superhydrophobicity. *Adv. Funct. Mater.* **2010**, *20* (4), 656−662.
(136) Pan, R.; Cai, M.; Liu, W.; Luo, X.; Chen, C.; Zhang, H.; Zhong, M. Extremely High Cassie−Baxter State Stability of Superhydrophobic Surfaces via Precisely Tunable Dual-Scale and Triple-Scale Micro−Nano Structures. *J. Mater. Chem. A* **2019**, *7* (30), 18050−18062.
(137) Li, J.; Jing, Z.; Zha, F.; Yang, Y.; Wang, Q.; Lei, Z. Facile Spray-Coating Process for the Fabrication of Tunable Adhesive Superhydrophobic Surfaces with Heterogeneous Chemical Compositions Used for Selective Transportation of Microdroplets with Different Volumes. *ACS Appl. Mater. Interfaces* **2014**, *6* (11), 8868−8877.
(138) Hu, Y.; Jiang, H.; Liu, J.; Li, Y.; Hou, X.; Li, C. Highly Compressible Magnetic Liquid Marbles Assembled from Hydrophobic Magnetic Chain-like Nanoparticles. *RSC Adv.* **2014**, *4* (7), 3162−3164.
(139) Liu, X.; Ye, Q.; Song, X.; Zhu, Y.; Cao, X.; Liang, Y.; Zhou, F. Responsive Wetting Transition on Superhydrophobic Surfaces with Sparsely Grafted Polymer Brushes. *Soft Matter* **2011**, *7* (2), 515−523.
(140) Liu, Z.; Fu, X.; Binks, B. P.; Shum, H. C. Mechanical Compression to Characterize the Robustness of Liquid Marbles. *Langmuir* **2015**, *31* (41), 11236−11242.
(141) Mele, E.; Bayer, I. S.; Nanni, G.; Heredia-Guerrero, J. A.; Ruffilli, R.; Ayadi, F.; Marini, L.; Cingolani, R.; Athanassiou, A. Biomimetic Approach for Liquid Encapsulation with Nanofibrillar Cloaks. *Langmuir* **2014**, *30* (10), 2896−2902.
(142) Rendos, A.; Alsharif, N.; Kim, B. L.; Brown, K. A. Elasticity and Failure of Liquid Marbles: Influence of Particle Coating and Marble Volume. *Soft Matter* **2017**, *13* (47), 8903−8909.
(143) Liu, Z.; Zhang, Y.; Chen, C.; Yang, T.; Wang, J.; Guo, L.; Liu, P.; Kong, T. Larger Stabilizing Particles Make Stronger Liquid Marble. *Small* **2019**, *15* (3), No. 1804549.
(144) Rane, Y.; Foster, E.; Moradiafrapoli, M.; Marston, J. O. Compressive Deformation of Liquid Marbles. *Powder Technol.* **2018**, *338*, 7−16.
(145) Polwaththe-Gallage, H. N.; Ooi, C. H.; Jin, J.; Sauret, E.; Nguyen, N. T.; Li, Z.; Gu, Y. The Stress-Strain Relationship of Liquid Marbles under Compression. *Appl. Phys. Lett.* **2019**, DOI: 10.1063/1.5079438.
(146) Azizian, S.; Fujii, S.; Kasahara, M.; Butt, H. J.; Kappl, M. Effect of Particle Morphology on Mechanical Properties of Liquid Marbles. *Adv. Powder Technol.* **2019**, *30*, 330.
(147) Huang, J.; Wang, Z.; Shi, H.; Li, X. Mechanical Robustness of Monolayer Nanoparticle-Covered Liquid Marbles. *Soft Matter* **2020**, *16*, 4632.
(148) Fujii, S.; Sawada, S.; Nakayama, S.; Kappl, M.; Ueno, K.; Shitajima, K.; Butt, H. J.; Nakamura, Y. Pressure-Sensitive Adhesive Powder. *Mater. Horizons* **2016**, *3* (1), 47−52.
(149) Sato, E.; Yuri, M.; Fujii, S.; Nishiyama, T.; Nakamura, Y.; Horibe, H. Liquid Marble Containing Degradable Polyperoxides for Adhesion Force-Changeable Pressure-Sensitive Adhesives. *RSC Adv.* **2016**, *6* (61), 56475−56481.
(150) Anyfantakis, M.; Jampani, V. S. R.; Kizhakidathazhath, R.; Binks, B. P.; Lagerwall, J. P. F. Responsive Photonic Liquid Marbles. *Angew. Chem.* **2020**, *132* (43), 19422−19429.
(151) Ukiwe, C.; Kwok, D. Y. On the Maximum Spreading Diameter of Impacting Droplets on Well-Prepared Solid Surfaces. *Langmuir* **2005**, *21* (2), 666−673.
(152) Wildeman, S.; Visser, C. W.; Sun, C.; Lohse, D. On the Spreading of Impacting Drops. *J. Fluid Mech.* **2016**, *805*, 636.
(153) Chandra, S.; Avedisian, C. T. On the Collision of a Droplet with a Solid Surface. *Proc. R. Soc. London. Ser. A Math. Phys. Sci.* **1991**, *432* (1884), 13−41.
(154) Clanet, C.; Béguin, C.; Richard, D.; Quéré, D. Maximal Deformation of an Impacting Drop. *J. Fluid Mech.* **1999**, *517*, 199−208.
(155) Lin, S.; Wang, Y.; Sun, L.; Mehrizi, A. A.; Jin, Y.; Chen, L. Experimental and Numerical Investigations on the Spreading Dynamics of Impinging Liquid Droplets on Diverse Wettable Surfaces. *Int. J. Multiph. Flow* **2022**, *153*, No. 104135.
(156) Padmanathan, A. M. D.; Ravi, A. S.; Choudhary, H.; Varanakkottu, S. N.; Dalvi, S. V. Predictive Framework for the Spreading of Liquid Drops and the Formation of Liquid Marbles on Hydrophobic Particle Bed. *Langmuir* **2019**, *35* (20), 6657−6668.
(157) Laan, N.; De Bruin, K. G.; Bartolo, D.; Josserand, C.; Bonn, D. Maximum Diameter of Impacting Liquid Droplets. *Phys. Rev. Appl.* **2014**, DOI: 10.1103/PhysRevApplied.2.044018.
(158) Šikalo, Š.; Marengo, M.; Tropea, C.; Ganić, E. N. Analysis of Impact of Droplets on Horizontal Surfaces. *Exp. Therm. Fluid Sci.* **2002**, *25* (7), 503−510.
(159) Kim, H.; Lee, C.; Kim, M. H.; Kim, J. Drop Impact Characteristics and Structure Effects of Hydrophobic Surfaces with Micro-and/or Nanoscaled Structures. *Langmuir* **2012**, *28* (30), 11250−11257.
(160) Lee, J. B.; Derome, D.; Guyer, R.; Carmeliet, J. Modeling the Maximum Spreading of Liquid Droplets Impacting Wetting and Nonwetting Surfaces. *Langmuir* **2016**, *32* (5), 1299−1308.
(161) Visser, C. W.; Tagawa, Y.; Sun, C.; Lohse, D. Microdroplet Impact at Very High Velocity. *Soft Matter* **2012**, *8* (41), 10732−10737.
(162) Marston, J. O.; Thoroddsen, S. T.; Ng, W. K.; Tan, R. B. H. H. Experimental Study of Liquid Drop Impact onto a Powder Surface. *Powder Technol.* **2010**, *203* (2), 223−236.
(163) Zhao, S. C.; De Jong, R.; Van Der Meer, D. Liquid-Grain Mixing Suppresses Droplet Spreading and Splashing during Impact. *Phys. Rev. Lett.* **2017**, DOI: 10.1103/PhysRevLett.118.054502.
(164) Umbanhowar, P.; Goldman, D. I. Granular Impact and the Critical Packing State. *Phys. Rev. E - Stat. Nonlinear, Soft Matter Phys.* **2010**, DOI: 10.1103/PhysRevE.82.010301.
(165) Nefzaoui, E.; Skurtys, O. Impact of a Liquid Drop on a Granular Medium: Inertia, Viscosity and Surface Tension Effects on the Drop Deformation. *Exp. Therm. Fluid Sci.* **2012**, *41*, 43−50.
(166) Khoufech, A.; Benali, M.; Saleh, K. Influence of Liquid Formulation and Impact Conditions on the Coating of Hydrophobic Surfaces. *Powder Technol.* **2015**, *270* (PB), 599−611.

https://doi.org/10.1021/acsomega.3c07657
ACS Omega 2024, 9, 12307−12330

(167) Bartolo, D.; Josserand, C.; Bonn, D. Retraction Dynamics of Aqueous Drops upon Impact on Non-Wetting Surfaces. *J. Fluid Mech.* **2005**, *545*, 329−338.
(168) Yarin, A. L. DROP IMPACT DYNAMICS: Splashing, Spreading, Receding, Bouncing.. *Ahh. Rev. Fluid Mechanics* **2005**, *38*, 159−192, DOI: 10.1146/annurev.fluid.38.050304.092144.
(169) Antonini, C.; Villa, F.; Bernagozzi, I.; Amirfazli, A.; Marengo, M. Drop Rebound after Impact: The Role of the Receding Contact Angle. *Langmuir* **2013**, *29* (52), 16045−16050.
(170) Šikalo, Š.; Tropea, C.; Ganić, E. N. Dynamic Wetting Angle of a Spreading Droplet. *Exp. Therm. Fluid Sci.* **2005**, *29* (7), 795−802.
(171) Vadillo, D. C.; Soucemarianadin, A.; Delattre, C.; Roux, D. C. D. Dynamic Contact Angle Effects onto the Maximum Drop Impact Spreading on Solid Surfaces. *Phys. Fluids* **2009**, *21* (12), 122002.
(172) Damak, M.; Hyder, M. N.; Varanasi, K. K. Enhancing Droplet Deposition through In-Situ Precipitation. *Nat. Commun.* **2016**, *7* (1), 12560.
(173) Wirth, W.; Storp, S.; Jacobsen, W. Mechanisms Controlling Leaf Retention of Agricultural Spray Solutions. *Pestic. Sci.* **1991**, *33*, 411.
(174) Aytouna, M.; Bartolo, D.; Wegdam, G.; Bonn, D.; Rafaï, S. Impact Dynamics of Surfactant Laden Drops: Dynamic Surface Tension Effects. *Exp. Fluids* **2010**, *48* (1), 49−57.
(175) Cruz, P. J.; De Breuck, P. P.; Rignanese, G. M.; Glinel, K.; Jonas, A. M. Influence of Roughness and Coating on the Rebound of Droplets on Fabrics. *Surfaces and Interfaces* **2023**, *36*, No. 102524.
(176) Liang, G.; Mudawar, I. Review of Drop Impact on Heated Walls. *Int. J. Heat Mass Transfer* **2017**, *106*, 103−126.
(177) McBride, S. A.; Girard, H. L.; Varanasi, K. K. Crystal Critters: Self-Ejection of Crystals from Heated, Superhydrophobic Surfaces. *Sci. Adv.* **2021**, *7* (18), 6960−6988.
(178) Bartolo, D.; Josserand, C.; Bonn, D. Singular Jets and Bubbles in Drop Impact. *Phys. Rev. Lett.* **2006**, *96* (12), No. 124501.
(179) Mao, T.; Kuhn, D. C. S.; Tran, H. Spread and Rebound of Liquid Droplets upon Impact on Flat Surfaces. *AIChE J.* **1997**, *43* (9), 2169−2179.
(180) Mao, T.; Kuhn, D. C. S.; Tran, H. Spread and Rebound of Liquid Droplets upon Impact on Flat Surfaces Spread and Rebound of Liquid Droplets upon Impact on Flat Surfaces. *AIChE J.* **1997**, *43* (9), 2169−2179.
(181) Tsai, P.; Pacheco, S.; Pirat, C.; Lefferts, L.; Lohse, D. Drop Impact upon Micro- and Nanostructured Superhydrophobic Surfaces. *Langmuir* **2009**, *25* (20), 12293−12298.
(182) Bergeron, V.; Bonn, D.; Martin, J. Y.; Vovelle, L. Controlling Droplet Deposition with Polymer Additives. *Nature* **2000**, *405* (6788), 772−775.
(183) Dhar, P.; Mishra, S. R.; Samanta, D. Onset of Rebound Suppression in Non-Newtonian Droplets Post-Impact on Superhydrophobic Surfaces. *Phys. Rev. Fluids* **2019**, *4* (10), No. 103303.
(184) Whitby, C. P.; Bian, X.; Sedev, R. Free Running Droplets on Packed Powder Beds. *AIP Conf. Proc.* **2013**, *1542* (1), 1043−1046.
(185) Lathia, R.; Dey Modak, C.; Sen, P. Suppression of Droplet Pinch-off by Early Onset of Interfacial Instability. *J. Colloid Interface Sci.* **2023**, *646*, 606−615.
(186) Marston, J. O.; Seville, J. P.; Cheun, Y. V.; Ingram, A.; Decent, S. P.; Simmons, M. J. Effect of Packing Fraction on Granular Jetting from Solid Sphere Entry into Aerated and Fluidized Beds. *Phys. Fluids* **2008**, *20* (2), 023301.
(187) Pritchard, J. R. J.; Chubynsky, M. V.; Marston, J. O.; Sprittles, J. E. Deformed Liquid Marble Formation: Experiments and Computational Modeling. *Phys. Rev. Fluids* **2021**, *6* (10), No. 104007.
(188) Katsuragi, H. Length and Time Scales of a Liquid Drop Impact and Penetration into a Granular Layer. *J. Fluid Mech.* **2011**, *675*, 552.
(189) McHale, G.; Newton, M. I.; Shirtcliffe, N. J. Water-Repellent Soil and Its Relationship to Granularity, Surface Roughness and Hydrophobicity: A Materials Science View. *Eur. J. Soil Sci.* **2005**, *56* (4), 445−452.
(190) McHale, G.; Shirtcliffe, N. J.; Newton, M. I.; Pyatt, F. B. Implications of Ideas on Super-Hydrophobicity for Water Repellent Soil. *Hydrol. Process.* **2007**, *21* (17), 2229−2238.
(191) Atherton, S.; Polak, D.; Hamlett, C. A. E.; Shirtcliffe, N. J.; McHale, G.; Ahn, S.; Doerr, S. H.; Bryant, R.; Newton, M. I. Drop Impact Behaviour on Alternately Hydrophobic and Hydrophilic Layered Bead Packs. *Chem. Eng. Res. Des.* **2016**, *110*, 200−208.
(192) Movasat, M.; Cruz, A. D. La; Tomac, I. Role of Hydrophobic Sand Particle Granularity on Water Droplet Post-Impact Dynamics. *Int. J. Multiph. Flow* **2023**, *167*, No. 104529.
(193) Yarin, A. L. L. DROP IMPACT DYNAMICS: Splashing, Spreading, Receding, Bouncing. *Annu. Rev. Fluid Mech.* **2006**, *38* (1), 159−192.
(194) Palacios, J.; Gómez, P.; Zanzi, C.; López, J.; Hernández, J. Experimental Study on the Splash/Deposition Limit in Drop Impact onto Solid Surfaces, ILASS − Europe 2010, 23rd Annual Conference on Liquid Atomization and Spray Systems, Brno, Czech Republic, September 2010.
(195) Xu, L.; Barcos, L.; Nagel, S. R. Splashing of Liquids: Interplay of Surface Roughness with Surrounding Gas. *Phys. Rev. E* **2007**, *76* (6), No. 066311.
(196) Smith, F. R.; Buntsma, N. C.; Brutin, D. Roughness Influence on Human Blood Drop Spreading and Splashing. *Langmuir* **2018**, *34*, 1143.
(197) Latka, A.; Boelens, A. M. P.; Nagel, S. R.; De Pablo, J. J. Drop Splashing Is Independent of Substrate Wetting. *Phys. Fluids* **2018**, *30* (2), No. 022105.
(198) Xu, L.; Zhang, W. W.; Nagel, S. R. Drop Splashing on a Dry Smooth Surface. *Phys. Rev. Lett.* **2005**, *94* (18), No. 184505.
(199) Xu, L. Liquid Drop Splashing on Smooth, Rough, and Textured Surfaces. *Phys. Rev. E - Stat. Nonlinear, Soft Matter Phys.* **2007**, *75* (5), 1−8.
(200) Vander Wal, R. L.; Berger, G. M.; Mozes, S. D. The Splash/Non-Splash Boundary upon a Dry Surface and Thin Fluid Film. *Exp. Fluids* **2006**, *40* (1), 53−59.
(201) Marmanis, H.; Thoroddsen, S. T. Scaling of the Fingering Pattern of an Impacting Drop. *Phys. Fluids* **1996**, *8* (6), 1344.
(202) Aziz, S. D.; Chandra, S. Impact, Recoil and Splashing of Molten Metal Droplets. *Int. J. Heat Mass Transfer* **2000**, *43* (16), 2841−2857.
(203) Lembach, A. N.; Tan, H. B.; Roisman, I. V.; Gambaryan-Roisman, T.; Zhang, Y.; Tropea, C.; Yarin, A. L. Drop Impact, Spreading, Splashing, and Penetration into Electrospun Nanofiber Mats. *Langmuir* **2010**, *26* (12), 9516−9523.
(204) Quetzeri-Santiago, M. A.; Yokoi, K.; Castrejón-Pita, A. A.; Castrejón-Pita, J. R. Role of the Dynamic Contact Angle on Splashing. *Phys. Rev. Lett.* **2019**, *122* (22), No. 228001.
(205) García-Geijo, P.; Riboux, G.; Gordillo, J. M. Role of Liquid Viscosity and of Air Entrapped on the Splashing of Drops Impacting over Superhydrophobic Substrates. *Phys. Rev. Fluids* **2022**, *7* (9), No. 093606.
(206) Palacios, J.; Hernández, J.; Gómez, P.; Zanzi, C.; López, J. Experimental Study of Splashing Patterns and the Splashing/Deposition Threshold in Drop Impacts onto Dry Smooth Solid Surfaces. *Exp. Therm. Fluid Sci.* **2013**, *44*, 571−582.
(207) Almohammadi, H.; Amirfazli, A. Droplet Impact: Viscosity and Wettability Effects on Splashing. *J. Colloid Interface Sci.* **2019**, *553*, 22−30.
(208) Esmaili, E.; Chen, Z. Y.; Pandey, A.; Kim, S.; Lee, S.; Jung, S. Corona Splashing Triggered by a Loose Monolayer of Particles. *Appl. Phys. Lett.* **2021**, *119* (17). DOI: 10.1063/5.0059466.
(209) Roy, P. K.; Legchenkova, I.; Shoval, S.; Bormashenko, E. Interfacial Crystallization within Janus Saline Marbles. *J. Phys. Chem. C* **2021**, *125* (2), 1414−1420.
(210) Zhao, Z.; Ling, C.; Wang, D.; Wang, J. X.; Saczek, J.; Pramana, S.; Sridhar, S.; Shang, J.; Xu, B. B.; Tsang, D. C. W.; et al. Liquid Marbles in Liquid. *Small* **2020**, *16* (37), No. 2002802.

https://doi.org/10.1021/acsomega.3c07657
ACS Omega 2024, 9, 12307−12330

(211) Mahmoudi Salehabad, S.; Azizian, S.; Fujii, S. Shape-Designable Liquid Marbles Stabilized by Gel Layer. *Langmuir* **2019**, *35* (27), 8950−8960.
(212) Katsuragi, H. Morphology Scaling of Drop Impact onto a Granular Layer. *Phys. Rev. Lett.* **2010**, DOI: 10.1103/PhysRevLett.104.218001.
(213) Zhao, R.; Zhang, Q.; Tjugito, H.; Cheng, X. Granular Impact Cratering by Liquid Drops: Understanding Raindrop Imprints through an Analogy to Asteroid Strikes. *Proc. Natl. Acad. Sci. U. S. A.* **2015**, *112* (2), 342−347.
(214) Walsh, A. M.; Holloway, K. E.; Habdas, P.; de Bruyn, J. R. Morphology and Scaling of Impact Craters in Granular Media. *Phys. Rev. Lett.* **2003**, DOI: 10.1103/PhysRevLett.91.104301.
(215) Holsapple, K. A.; Schmidt, R. M. Point Source Solutions and Coupling Parameters in Cratering Mechanics. *J. Geophys. Res.* **1987**, *92*, 6350.
(216) De Jong, R.; Zhao, S. C.; Garcia-Gonzalez, D.; Verduijn, G.; Van Der Meer, D. Impact Cratering in Sand: Comparing Solid and Liquid Intruders. *Soft Matter* **2021**, *17* (1), 120−125.
(217) Ye, X.; Van Der Meer, D. Hydrogel Sphere Impact Cratering, Spreading and Bouncing on Granular Media. *J. Fluid Mech.* **2021**, *929*, No. A24.
(218) Delon, G.; Terwagne, D.; Dorbolo, S.; Vandewalle, N.; Caps, H. Impact of Liquid Droplets on Granular Media. *Phys. Rev. E - Stat. Nonlinear, Soft Matter Phys.* **2011**, DOI: 10.1103/PhysRevE.84.046320.
(219) Zhao, S. C.; De Jong, R.; Van Der Meer, D. Raindrop Impact on Sand: A Dynamic Explanation of Crater Morphologies. *Soft Matter* **2015**, *11* (33), 6562−6568.
(220) Emady, H. N.; Kayrak-Talay, D.; Schwerin, W. C.; Litster, J. D. Granule Formation Mechanisms and Morphology from Single Drop Impact on Powder Beds. *Powder Technol.* **2011**, *212* (1), 69−79.
(221) De Jong, R.; Zhao, S. C.; Van Der Meer, D. Crater Formation during Raindrop Impact on Sand. *Phys. Rev. E* **2017**, *95* (4), 1−8.
(222) Zhang, Q.; Gao, M.; Zhao, R.; Cheng, X. Scaling of Liquid-Drop Impact Craters in Wet Granular Media. *Phys. Rev. E - Stat. Nonlinear, Soft Matter Phys.* **2015**, DOI: 10.1103/PhysRevE.92.042205.
(223) Matsuda, Y.; Kamiya, R.; Yamaguchi, H.; Uchiyama, T. Dynamics of Impact Cratering on Granular Bed by Hydrogel Sphere. *Phys. Fluids* **2020**, *32* (6), No. 067112.
(224) Ahn, S.; Doerr, S. H.; Douglas, P.; Bryant, R.; Hamlett, C. A. E.; Mchale, G.; Newton, M. I.; Shirtcliffe, N. J. Effects of Hydrophobicity on Splash Erosion of Model Soil Particles by a Single Water Drop Impact. *Earth Surf. Process. Landforms* **2013**, *38* (11), 1225−1233.
(225) Wyser, E.; Carrea, D.; Jaboyedoff, M.; Pudasaini, S. P. Cratering Response during Droplet Impacts on Granular Beds. *Eur. Phys. J. E 2019 428* **2019**, *42* (8), 1−11.
(226) De Vet, S. J.; De Bruyn, J. R. Shape of Impact Craters in Granular Media. *Phys. Rev. E - Stat. Nonlinear, Soft Matter Phys.* **2007**, *76* (4), No. 041306.
(227) Marston, J. O.; Zhu, Y.; Vakarelski, I. U.; Thoroddsen, S. T. Deformed Liquid Marbles: Freezing Drop Oscillations with Powders. *Powder Technol.* **2012**, *228*, 424−428.
(228) Supakar, T.; Kumar, A.; Marston, J. O. Impact Dynamics of Particle-Coated Droplets. *Phys. Rev. E* **2017**, *95* (1), 1−10.
(229) Li, X.; Wang, Y.; Yang, Y.; Wang, S.; Zang, D.; Geng, X. Dynamic Behavior of Droplets under Interfacial Jamming of Nanoparticles. *Appl. Phys. Lett.* **2018**, *113* (13), No. 133702.
(230) Geyer, F.; Asaumi, Y.; Vollmer, D.; Butt, H. J.; Nakamura, Y.; Fujii, S. Polyhedral Liquid Marbles. *Adv. Funct. Mater.* **2019**, *29* (25), No. 1808826.
(231) Tenjimbayashi, M.; Samitsu, S.; Watanabe, Y.; Nakamura, Y.; Naito, M. Liquid Marble Patchwork on Super-Repellent Surface. *Adv. Funct. Mater.* **2021**, *31* (21), No. 2010957.
(232) Li, X.; Shi, H.; Wang, Y.; Wang, R.; Huang, S.; Huang, J.; Geng, X.; Zang, D. Liquid Shaping Based on Liquid Pancakes. *Adv. Mater. Interfaces* **2018**, *5* (2), No. 1701139.
(233) Subramaniam, A. B.; Abkarian, M.; Mahadevan, L.; Stone, H. A. Non-Spherical Bubbles. *Nat. 2005 4387070* **2005**, *438* (7070), 930−930.
(234) Cui, M.; Emrick, T.; Russell, T. P. Stabilizing Liquid Drops in Nonequilibrium Shapes by the Interfacial Jamming of Nanoparticles. *Science (80-.).* **2013**, *342* (6157), 460−463.
(235) Asaumi, Y.; Rey, M.; Oyama, K.; Vogel, N.; Hirai, T.; Nakamura, Y.; Fujii, S. Effect of Stabilizing Particle Size on the Structure and Properties of Liquid Marbles. *Langmuir* **2020**, *36*, 13274.
(236) Lee, A. C. S.; Sojka, P. E. Drop Impact and Agglomeration under Static Powder Bed Conditions. *AIChE J.* **2012**, *58* (1), 79−86.
(237) Josserand, C.; Thoroddsen, S. T. Drop Impact on a Solid Surface. *Ann. Ren. Fluid Mechanics* **2016**, *48*, 365−391, DOI: 10.1146/annurev-fluid-122414-034401.
(238) Lekshmi, B. S.; Yadav, A. S.; Ranganathan, P.; Varanakkottu, S. N. Simple and Continuous Fabrication of Janus Liquid Marbles with Tunable Particle Coverage Based on Controlled Droplet Impact. *Langmuir* **2020**, *36* (50), 15396−15402.

https://doi.org/10.1021/acsomega.3c07657
ACS Omega 2024, 9, 12307−12330